International Journal of
Molecular Sciences

MDPI

Review

Photochemical Haze Formation on Titan and Uranus: A Comparative Review

David Dubois [1,2]

[1] NASA Ames Research Center, MS 245-6, Moffett Field, CA 94035, USA; david.f.dubois@nasa.gov
[2] Bay Area Environmental Research Institute, Moffett Field, CA 94035, USA

Abstract

The formation and evolution of haze layers in planetary atmospheres play a critical role in shaping their chemical composition, radiative balance, and optical properties. In the outer solar system, the atmospheres of Titan and the giant planets exhibit a wide range of compositional and seasonal variability, creating environments favorable for the production of complex organic molecules under low-temperature conditions. Among them, Uranus—the smallest of the ice giants—has, since Voyager 2, emerged as a compelling target for future exploration due to unanswered questions regarding the composition and structure of its atmosphere, as well as its ring system and diverse icy moon population (which includes four possible ocean worlds). Titan, as the only moon to harbor a dense atmosphere, presents some of the most complex and unique organics found in the solar system. Central to the production of these organics are chemical processes driven by low-energy photons and electrons (<50 eV), which initiate reaction pathways leading to the formation of organic species and gas phase precursors to high-molecular-weight compounds, including aerosols. These aerosols, in turn, remain susceptible to further processing by low-energy UV radiation as they are transported from the upper atmosphere to the lower stratosphere and troposphere where condensation occurs. In this review, I aim to summarize the current understanding of low-energy (<50 eV) photon- and electron-induced chemistry, drawing on decades of insights from studies of Titan, with the objective of evaluating the relevance and extent of these processes on Uranus in anticipation of future observational and in situ exploration.

Keywords: solar system; Titan; Uranus; giant planets; atmospheres; ion-neutral reactions; haze formation; astrochemistry

Academic Editor: Oleg N. Ulenikov

Received: 12 June 2025
Revised: 26 July 2025
Accepted: 1 August 2025
Published: 4 August 2025

Citation: Dubois, D. Photochemical Haze Formation on Titan and Uranus: A Comparative Review. *Int. J. Mol. Sci.* **2025**, *26*, 7531. https://doi.org/10.3390/ijms26157531

1. Introduction

In the four decades since Voyager 1 and Voyager 2 swept past all four gas giants, modelers, astronomers, and experimentalists have been incentivized to come one step closer to examining the outer planets and, ultimately, Uranus and Neptune. While the Jovian and Kronian systems have been receiving increased scrutiny, Uranus and Neptune remain the final frontiers of planetary exploration in our solar system. Recognized as a flagship mission top priority for the next decade, the selection of the Uranus Orbiter Probe (UOP) by the *Decadal Strategy for Planetary Science and Astrobiology 2023–2032* [1] illustrates a renewed interest in the next H_2-dominated planet. This window offers an opportunity to utilize decades of knowledge obtained from Jupiter to Saturn and the moons of these planets, as well as instrument development which could prove useful to characterize the atmospheres of Uranus or Neptune. As defined in [1], UOP would target fundamental questions about the origin and evolution of our solar system and

the dynamics of chemical disequilibria across the atmosphere (Q7.1c), the chemical and physical processes influencing haze formation (Q7.3d), local ion/neutral composition (Q7.4d), and seasonal effects triggering atmospheric chemistry and variability in haze production (Q7.5c). For the latter topic, supportive laboratory and numerical studies of high- and low-pressure chemistry, reaction rates, and photochemistry will especially be relevant to improve our understanding of Uranus' atmospheric dynamics and chemistry.

Closer than Uranus, Saturn's largest moon Titan is the only moon in the solar system with a dense atmosphere. This atmosphere contains numerous organic molecules as well as detached haze layers resulting from intense photochemical activity in the upper atmosphere. The opaque organic haze hides a geologically rich surface made of dunes, craters, and liquid methane and ethane lakes. The Cassini-Huygens mission which arrived at Titan in 2004 (and Huygens landing on Titan in 2005), unmasked for 13 years several of Titan's characteristics until the end-of-mission in 2017. After almost 350 years since its discovery by Christiaan Huygens in 1655, many of Titan's secrets were about to be unveiled [2–6]. The unprecedented data collected by Cassini and Huygens at Titan unveiled, over a large spectrum covering the UV up to radio wavelengths, many of the atmosphere's physical, chemical, thermal, and transport characteristics from the surface to the thermosphere. The Cassini-Huygens mission has deepened our understanding of the role of photochemistry on haze formation, benefiting from holistic experimental, modeling, and observational studies [6–10]. Investigations have shed light on the seasonal variations in temperature and cloud coverage, the structure of the detached haze layer, and the role of neutral-ion reactivity on the nucleation and growth of high-altitude aerosols. Still, many open questions prevail [9] and in addition to newer observations conducted to expand our knowledge of Titan's chemical inventory, Cassini's data heritage remains vast enough to probe for many years to come [9,11,12].

Across the four gas giant planets' H_2-dominated atmospheres, photochemical process are mainly driven by ultraviolet (UV) photons, magnetospheric energetic electrons and auroral deposition, galactic cosmic rays (GCR), and lightning-induced chemistry. The chemical inventory in these atmospheres directly depends on the source and intensity of photon deposition, and the photon penetration depth (see sections hereafter). In this context, the focus of this review will be on studies that have explored photochemical processes within three wavelength regions spanning UV photon energies from 3.1 to 50 eV (Table 1); this is a photon region at the source of fundamental dissociative and ionizing processes, resulting in the molecular and atmospheric diversity observed on Titan and Uranus. Region 1 contains Far-Ultraviolet (FUV) photons, Region 2 corresponds to Lyman-α radiation, and Region 3 contains more energetic Extreme-Ultraviolet (EUV) photons. Studies investigating processes induced by low-energy (<50 eV) chemistry will be reviewed according to the wavelength range as classified in Table 1.

Table 1. Spectral regions with associated energy (eV) and wavelength ranges.

	Region 1	***Region 2***	***Region 3***
	Near/Far-UV (400–121.6 nm)	**Lyman-α** (121.6 nm)	**EUV/VUV** (121.6–25 nm)
Energy range (eV)	3.1–10.2	10.2	10.2–49.6

Although the atmospheric compositions of both Titan and Uranus are distinct, decades of Titan research might help in identifying areas and techniques for both bodies needing further scrutiny into their atmospheric photochemical processes. Furthermore, the second most abundant category of exoplanets in the most comprehensive catalogues consists of mini-Neptune and Neptune exoplanets. These exoplanets have sizes of $2 < R_{\oplus} < 6$, but the

definition of this size classification itself relies on planets (i.e., Uranus and Neptune) whose characteristics themselves are poorly known. As such, further exploring Uranus (and Neptune) will not only help in exoplanetary characterization, but also in our understanding of planetary formation and the solar system's evolution. Within our solar system, all four hydrogen-helium-rich planets hold most of the planetary mass of the solar system. Both ice giants hold a combined total of 41 moons. Our understanding of the formation and evolution of these systems relies on planetary formation and hydrodynamic models [13,14].

This review is structured into four sections as follow:

- Section 2 will include a review of the atmospheric and radiative environments of the ice giants with an emphasis on Uranus and how they differ from Titan in the Saturnian system. In addition, I will survey the current state-of-the-art body of knowledge of their chemical inventories.
- Section 3 will include a review of the state of knowledge of low-energy (<50 eV) photochemistry-induced mechanisms on Titan and Uranus, covering observations and in situ measurements, experimental simulations of gas phase and condensed state chemistry, photochemical modeling, dicationic chemistry, and recent advances in quantum chemical calculations. Important aspects of branching ratio determination will also be discussed.
- Section 4 will be dedicated to negative ions. Discoveries pertaining to negative ion chemistry on Titan deserve their own section, as their participation in molecular and haze growth requiring photochemical and radiative processes has proven to be substantial.
- Section 5 will conclude with a summary of potential future investigations needed to probe Uranus and prepare for upcoming studies before future missions to the gas giants.

2. The Chemical and Radiative Environments of Titan and the Ice Giants

2.1. Ice Giants: General Considerations

Uranus and Neptune (the "ice giants") are the least explored planets of our solar system. To date, Voyager 2 is the only mission to have flown by anywhere close to Uranus and Neptune, at a distance of 4 $R_{♅}$ and 1/5 $R_{♆}$, respectively. For the first time, these missions revealed unprecedented imagery and data of not just the two farthest gaseous planets, but also 16 new moons and 2 new rings (Figure 1). Since Voyager 2 departed Neptune's vicinity in 1989, no other dedicated spacecraft has gone back. The ice giants stand apart from Jupiter and Saturn in their own category. On a compositional level, Uranus and Neptune both contain multiple suspected cloud layers stratified in CH_4, H_2S, NH_4SH, H_2O, and NH_3. The temperature profiles in these planets are poorly constrained and usually assumed to follow a standard moist adiabatic and well-defined profile [15]. Radio occultation and mid-infrared measurements supported by global-average thermochemical equilibrium modeling helped in characterizing the atmospheric regions of these planets [16–21].

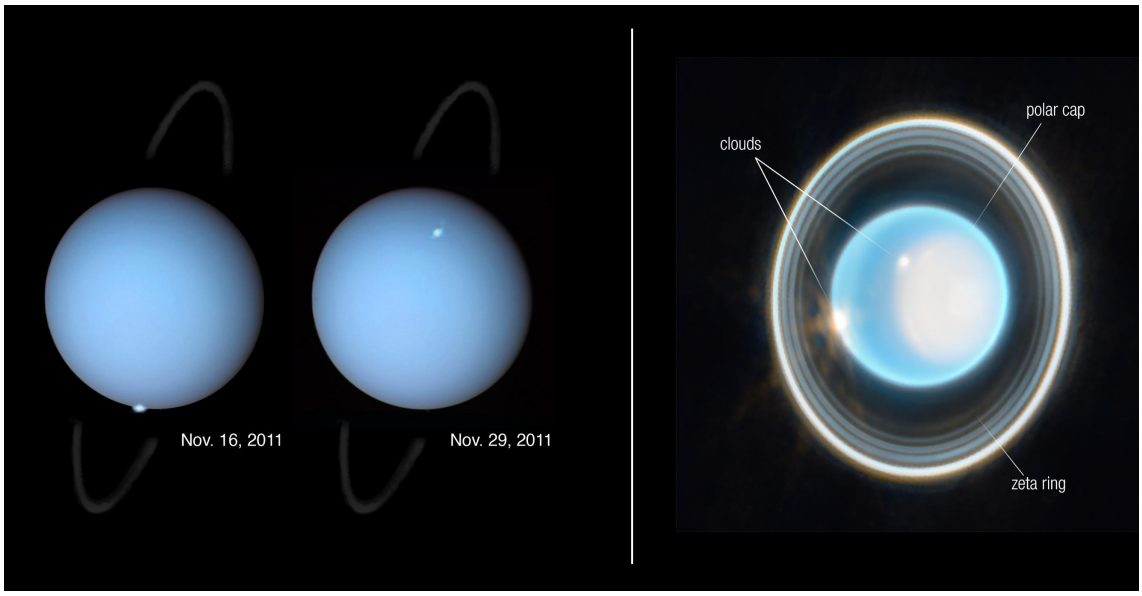

Figure 1. Left: Composite image of Uranus combining auroral observations as seen in FUV by HTS/STIS for the first time in November 2011 [22], with the planet's blue disk seen by Voyager 2 in 1986. The faint ring system observed by the Gemini Observatory observed in 2011 is also overlaid. **Right**: JWST/NIRCam image taken on February 6, 2023. Bright sun-facing polar cap and multiple bright cloud systems can be seen. The planet's complex 13-ring system was also captured by NIRCam with the innermost and optically thin ζ ring being visible. Image credits: NASA, ESA, and L. Lamy (Observatory of Paris, CNRS, CNES); NASA, ESA, CSA, STScI, Joseph DePasquale (STScI).

A deep troposphere resides below the 0.1 bar pressure level, where temperatures are predicted to range from ~200 K at the 10 bar level down to 50–60 K at 0.1 bar. Marking the tropopause at 0.1 bar (50 km) in both planets, the temperature inversion sets the boundary between the troposphere and the stratosphere wherein temperatures substantially increase with increasing altitude up to the thermospheric boundary located at the 1 µbar level (550 km). At these altitudes, Uranus is already much warmer than Neptune (350 K vs. 180 K). In the upper atmosphere extending up to 6000 km in the case of Uranus, Voyager 2 measurements taken by the Ultraviolet Spectrometer (UVS) show temperatures reaching 750 K near the exobase [23]. The Neptunian exobase is located around 4000 km [24]. Notwithstanding large distances from the Sun, both upper atmospheres are hotter than Saturn's upper atmosphere, while Neptune's is almost as hot as Jupiter's, when considering solar heating alone [23]. Interestingly, Uranus and Neptune have both undergone an important cooling phase of their upper atmospheres since Voyager's flybys [23,25]. Energetics and dynamics mechanisms (high-energy particle ionization, auroral processes, photoionization, solar and seasonal cycles) have been investigated to understand the intense cooling of Uranus's atmosphere but have fallen short of combining all the complex seasonal, photochemical, orbital, and dynamical processes shaping into one cohesive theory ([23], *and references therein*). While both planets share similar temperature and atmospheric profiles, they also exhibit distinct additional characteristics. Vertical mixing is, in the standard models, assumed to be negligible at Uranus, while much more vigorous mixing is present at Neptune [15,20,26]. Eddy diffusion (K_z) has been described as "sluggish" by [27] with equatorial values at the homopause ranging from 3000 to 10,000 cm^2 s^{-1} [17,18,27–29]. Earlier modeling had placed vertical mixing even lower <100 mbar at 200 cm^2 s^{-1}. Eddy diffusion is the main transport mechanism for vertical mixing but its coefficient is an important free parameter in 1D photochemical models. However, the assumption of a temperature profile which follows a moist adiabatic lapse rate does not fully reproduce the likelihood that latitudinal variations due to meridional circulation, super-adiabatic conditions, and turbulent

updrafts/downdrafts may strongly influence the distribution of photochemically produced species in the atmosphere [15,21]. Coupled to auroral processes and auroral driven Joule heating, and EUV photoionization, the unique orbital geometry of Uranus (i.e., an extreme axial tilt of 97.8°) makes it a unique planet in the solar system. Although far from the Sun, solar spectrum irradiance (SSI) may reach $\sim 10^{-5}$–10^{-4} W m^{-2} nm^{-1} at Lyman-alpha (Ly-α) wavelengths at the top of Uranus's atmosphere (Figure 2). In addition, Uranus does not have an internal heating source, unlike Neptune [30], and the lack of understanding in the radiant energy budget of Uranus has made elucidating the planet's weather and dynamical patterns difficult. However, recent modeling studies spanning the entire orbital period of Uranus have shed light on its internal heat flux and shown that Uranus does, in fact, possess a relatively significant internal heat source. This internal heat-to-absorbed solar power ratio is still much lower than that of the other gas giants [31]. More future studies are needed to resolve these discrepancies between models and observations [23].

2.2. The Atmosphere of Uranus

The atmosphere of Uranus has a mean molecular weight of around 2.3 which increases to 3.1 deeper in the troposphere below 1 bar where CH_4 reaches a near-constant mixing ratio of ~3% [15,19,32]. The intensity of solar EUV across the solar system decreases as the square of solar distance, where we find a solar constant of ~14.8 W m^{-2} at the Saturnian system and 3.7 W m^{-2} at Uranus (Table 2). EUV intensity in the 90–110 nm range (11.27–13.78 eV, Region 3, Table 1) falls at 0.21 kR and 0.05 kR, respectively. Presented differently, Voyager 2 UVS measurements of FUV reflectance at the Uranian subsolar point (i.e., close to the rotation axis) by [33] helped constrain the CH_4 column abundance even before the closest approach. At the same time, occultation experiments helped quantify the column abundances of H_2, H, and C_2H_2 [34]. These occultation measurements found that the opacity could be explained by the dominating presence of Rayleigh scattering of H_2 along with the presence of a Raman line at 1280 Å and C_2H_2 absorption near 1300 Å and 1500 Å [27,33]. More recently, Ref. [22] conducted the first Earth-based detection of an auroral event (transient emissions on the order of 1–2 kR) at Uranus, observed in the FUV in November 2011 during an intense solar wind event. These observations clearly indicated that there exist variations in the configuration between the solar wind and the magnetosphere, and therefore the thermal and compositional structure of the upper atmosphere. Later measurements by the Hubble Space Telescope (HST) permitted a re-analysis of Voyager 2's albedo measurements from [35], which brought down its value from ~20–30% to 5–10% between 135 and 155 nm (8.0–9.19 eV, Region 1, Table 1) [36]. The emission features studied therein would have required an estimated energy flux of the precipitating electrons of 0.04–0.07 erg cm^{-2} s^{-1}, but sensitivity shortcomings prevented any determination of their actual energy in the 20 eV–20 keV range. Nonetheless, this first Earth-based detection of a transient auroral H_2 emission came in good agreement with the Voyager 2-era disk average flux upper limit of 0.008 erg cm^{-2} s^{-1} by [37]. The modeled H_2 spectrum resulting from solar photons and precipitating electrons considered low-energy (centered at 20 eV) and higher energy (3 keV) electrons. The calculated χ^2 dependence of the precipitating flux showed little difference between these two energies and that one single transient event would have caused a total electron flux enhancement by a factor of 4–9 [36]. Overall, both Voyager 2 and Earth-based observations have contributed to a better understanding of auroral and photochemical events in the upper atmosphere of Uranus. However, we are still far from an accurate global picture involving complex latitudinal, temperature profile variations, hydrocarbon contributions, magnetospheric configuration, and accurate knowledge of solar FUV/EUV fluxes [38]. As such, a more accurate description of these fluxes (extrapolating also into more energetic X-ray fluxes)

will ultimately help in better characterizing exoplanet environments and their atmospheric composition [38–41].

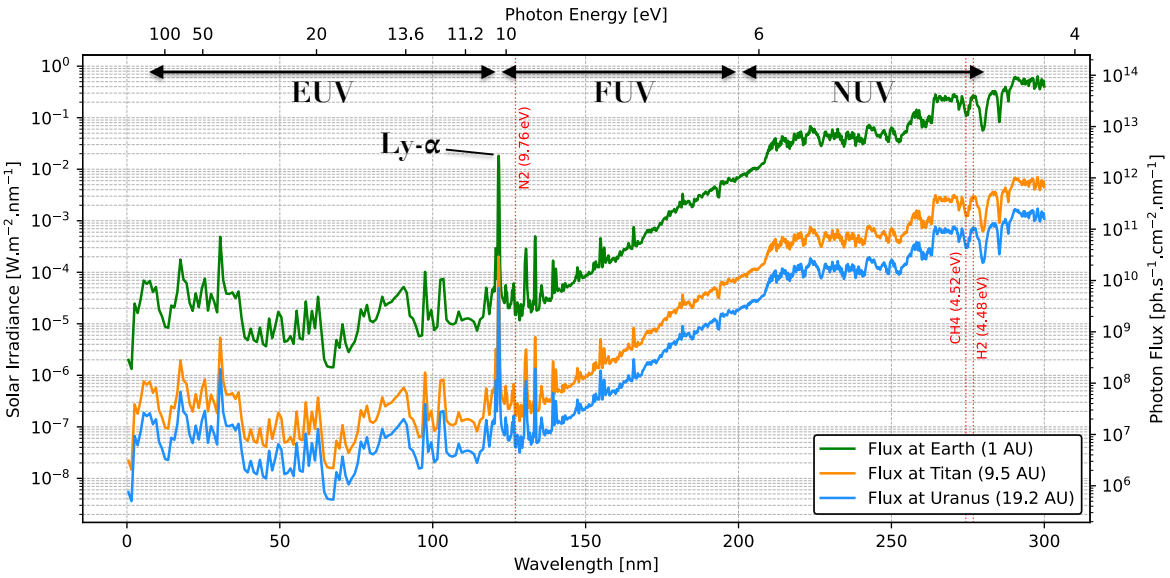

Figure 2. Disk-integrated high-resolution solar spectrum irradiance measured by SOLAR-HRS at Earth (1 AU) in green shown between 0.5 nm and 300 nm (data obtained with permission from [42]). The data, measured in 2022, represents a reference of a solar minimum spectrum with a spectral resolution < 1.0 nm. The spectrum is also scaled at Titan (9.5 AU) in orange and Uranus (19.2 AU) in blue here for comparison, decreasing at a scale of $1/r^2$. The intense Ly-α band can be seen at 121.6 nm, and red dotted lines correspond to the dissociative energy thresholds for N_2, CH_4, and H_2.

Table 2. Planetary parameters and solar activity measured by Voyager 2 at Saturn, Titan, and Uranus.

	Mass ($M_\oplus$)	Solar Constant (W m^{-2})	EUV Intensity (kR), 90–110 nm	T (1 bar Level) in Kelvin	Mean Molecular Weight
Titan	0.023	14.8	0.21	94	27.8
Saturn	95.2	14.8	0.21	134–145	2.0
Uranus	14.5	3.7	0.05	76–86	2.3

See [19,20,26] for references.

The first recorded molecular detection in Uranus occurred in 1869 by [43]: *"Dans le vert et dans le bleu il y a deux raies très-larges et très-noires"*. Unbeknownst to the astronomer and priest that this detection was in fact that of molecular hydrogen, this was followed by observations of unresolved faint bands by [44]. Then, *"The remarkable absorption taking place at Uranus shows itself in six strong lines"* [44,45]. This first set of two observations acquired very faint bands, but it was not until 1934 that the first observations firmly detected CH_4 as being the first confirmed compound in the atmosphere [46]. Eighteen years later, the H_2 ro-vibrational band at 8270 Å was discovered [47], and nearly thirty-four years later, accurate measurements of the H_2:He mole fraction were conducted and trace species were discovered by the International Ultraviolet Explorer [48] and Voyager 2 [49]. At present, 9 neutral molecules have been directly detected in the atmosphere of Uranus (see Table 3 for an elemental composition comparison between Uranus and Titan).

Table 3. Summary of all the directly detected neutral molecules in the atmospheres of Titan and Uranus [10,46–54].

Atoms	C		N		O		Other	
	Titan	**Uranus**	**Titan**	**Uranus**	**Titan**	**Uranus**	**Titan**	**Uranus**
1	CH_4	CH_4	HCN, HNC, CH_3CN, HC_3N, C_3H_3N, C_3H_5N, C_4H_3N	-	H_2O, CO	CO	-	H_2, H_2S
2	C_2H_2, C_2H_4, C_2H_6	C_2H_2, C_2H_6	N_2, C_2N_2	-	CO_2	CO_2	-	-
3	C_3H_2, C_3H_4, C_3H_6, C_3H_8	C_3H_4	-	-	-	-	-	-
4	C_4H_2	C_4H_2	-	-	-	-	-	-
5	-	-	-	-	-	-	-	-
6	C_6H_6	-	-	-	-	-	-	-

The atmosphere of Uranus starts with a deep troposphere which rises up to 1 bar, and whose composition and structure are still, to a large extent, poorly known [15,21]. CH_4 is in abundance and drives the moist convection in the troposphere, before it condenses due to the cold temperatures near the tropopause (1–1.5 bar). In models assuming a temperature profile following a moist adiabat, all expected CH_4, H_2S, NH_4SH, and H_2O-NH_3 species form stratified, well-defined cloud decks below 1 bar (Figure 3). Methane, like all other species, display latitudinal and temporal variations and as a result are important indications of underlying seasonal and/or vertical transport [18,21,55]. Indeed, as explained in [21], tropospheric updraft of methane and other hydrocarbons is unlikely given the cold trap at ∼50 K. However, mechanisms such as mid-latitude tropospheric updraft could in theory transport CH_4-rich air mass up into the stratosphere. Or, adiabatic warming may occur, thus moving subsiding air from the stratosphere into the troposphere [18,56] (a similar seasonally driven stratospheric circulation was seen on Titan, discussed later). Modeling of the visible/near-infrared reflectivity of the haze profile on Uranus includes several uncertainties but was recently studied by [57]. Their conclusion was that the atmosphere consists of three "detached" haze layers. (1) A vertically extended photochemical haze layer $< 10^{-2}$ bar which is produced in the lower to mid stratosphere. Haze particle are then relatively mixed to lower altitudes by Eddy diffusion. (2) Right above the CH_4 condensation altitude at ∼1 bar, haze particles of moderate size (∼1 μm) constitute a thin but highly opaque cloud structure composed of an important mixture of CH_4 ice and photochemically produced particles, absorbent of UV and long-wavelength photons. It is at this level that ice/haze particles are expected to act as cloud condensation nuclei (CCN). (3) Finally, a deeper and darker aerosol layer for P > 5–7 bar would be consistent with the presence of an H_2S-based layer mixed with photochemically generated aerosols and other ices. The modeled haze particles are predicted to scatter light at 500 nm while absorbing photons at longer wavelengths. Future experimental and numerical studies of the optical and physico-chemical properties of these particles would help in constraining the vertical structure of Uranus' atmosphere which remains largely uncertain. Support from telescopic observations is ongoing [58] and recent surveys using the Lowell Observatory and HST have highlighted the dependency of cloud brightness variations with CH_4 distributions and orbital position [59].

A number of species such as HCN, PH_3, GeH_4, HCl, and CH_3SH expected to be in disequilibrium have been speculated from thermochemical modeling to survive in the upper troposphere, thus importantly bridging the deep troposphere composition with

the stratosphere [20]. There are however many uncertainties surrounding this chemistry such as: knowledge of the deep tropospheric temperature profile, ice nucleation at low temperature, kilobar-level and high-temperature reactions rates, diffusion effects, and non-ideal gas behavior, all of which are factors of uncertainty that have been highlighted in [20]. Above the 1 bar pressure (Figure 3), the stratosphere extends up to ~1 µbar where temperatures rapidly reach 300 K, following the moist adiabat, and finally reach 750 K at the exobase [18]. This vertical structure interpretation is almost certainly erroneous for the reasons mentioned previously, and the reality is likely to involve many altitudinal, latitudinal, and seasonal variations [15]. These atmospheric parameters will regulate the distribution of species in the atmosphere, and these species will also influence the cloud structure and haze formation of the planet. Therefore, it is crucial to obtain a better understanding of the chemical inventory and physico-chemical processes in Uranus.

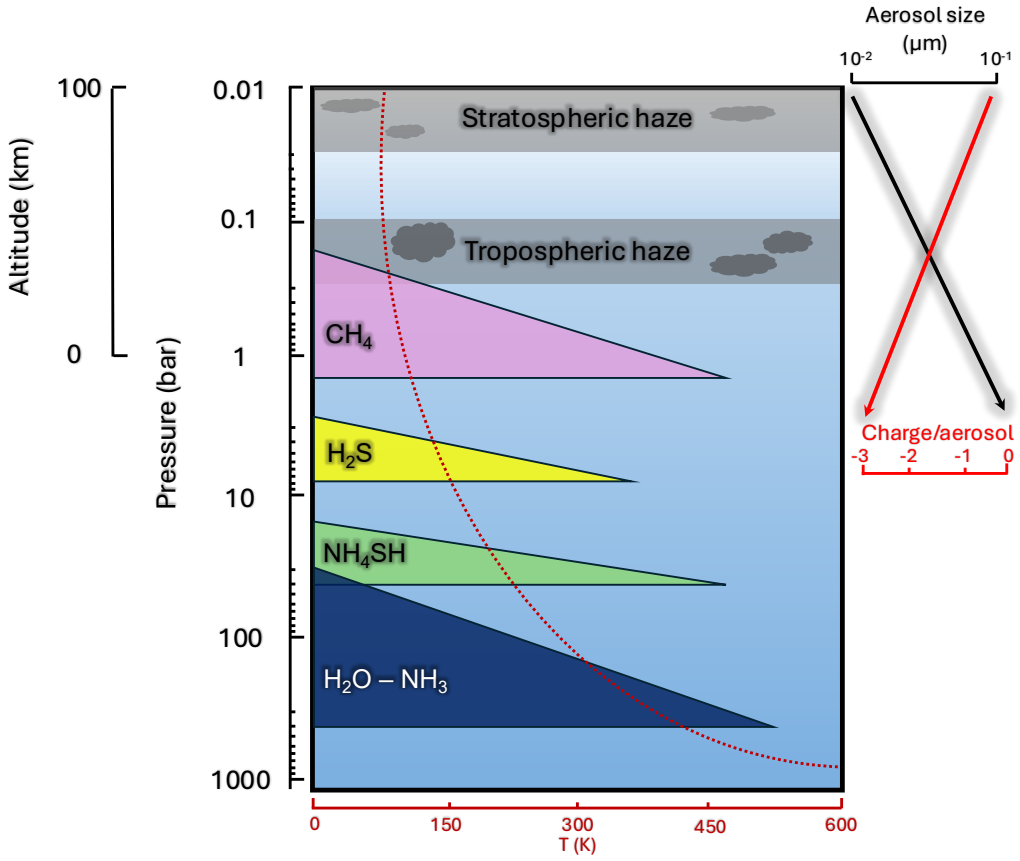

Figure 3. Standard picture schematic of the atmospheric profile of Uranus with the tropospheric and stratospheric haze layers, the CH_4, H_2S, NH_4SH, and H_2O-NH_3 cloud decks, and the approximate temperature profile [15,18–20,60,61]. The general, approximate trends across the haze layers for aerosol particle size distribution (in µm), and the distribution of the mean charge per aerosol from [62] at altitudes of 0.01–3 bar are also given.

2.3. Chemical Inventory in Uranus

This section will focus on the available inventory of detected species in the atmospheric column of Uranus. The origin and photolytical evolution of the species are still largely unknown, and as pointed out in [63] the differences observed with the other gas giants may result from different production/loss photolytic rates, variations in atmospheric mixing, extent of ion-neutral chemistry, auroral conditions, and exogenic material influx. To date, stratospheric column abundances have been measured for a total of 9 neutral molecules and one isotopic D/H (measured in H_2) with a value of 4.4×10^{-5} (Table 4). They are composed

of alkanes (CH_4, C_2H_6), alkenes (C_2H_4), alkynes (C_2H_2, C_3H_4, C_4H_2), and oxygenated molecules (CO, CO_2, and H_2O). Since no dedicated mission has yet flown to Uranus, new molecular discoveries happen at an irregular pace with long-term windows that depend on telescopic observations [64]. However, the benefits of a descending probe into the Uranian atmosphere are undeniable and would increase our understanding of the chemical, radiative, and optical properties of the atmosphere [63,64]. Such an in situ study would help us constrain the gas and haze composition with the energy deposition distribution in the atmosphere.

Table 4. Atmospheric gas phase composition in the stratospheres of Titan, Saturn, and Uranus.

	Stratosphere			
Species	**Titan**	**Saturn**	**Uranus**	**Ref.**
CH_4	1–2%	4.7×10^{-3}	16 ppm	[17,65,66]
C_2H_2	2.97×10^{-6}	1×10^{-6}	0.25 ppm	[67–70]
C_2H_4	1.2×10^{-7}	5.9×10^{-7}	$<2 \times 10^{-14}$	[17,70,71]
C_2H_6	7.3×10^{-6}	1×10^{-5}	0.13 ppm	[17,67–70]
C_3H_4	4.8×10^{-9}	1×10^{-9}	0.36 ppb	[17,70,72]
C_4H_2	1.12×10^{-9}	7×10^{-9}	0.13 ppb	[17,70,72]
CO_2	1.1×10^{-8}	4.5×10^{-10}	0.08 ppb	[17,70,73]
CO	4.7×10^{-5}	2.5×10^{-8}	6 ppb	[17,70,74]
H_2O	4.5×10^{-10}	1.1 ppb	3.8 ppb	[20,70,75]
D/H (in H_2/C_2H_2)	2.1×10^{-4}	2.1×10^{-5}	4.4×10^{-5}	[20,76,77]

Note: Only species shared in common and detected in all three atmospheres are shown here. For Titan, the averaged values were taken near the equator by CIRS [70]. Saturn measurements are approximate and derived from CIRS limb data near 400 km [69,72]. Abundances represented here are generally given at or near the mbar pressure level.

Multiple photochemical models have been developed, often studied in tandem with Neptune, to understand the global-averaged hydrocarbon distribution on both planets [17,78–84]. Generally, they did not however include seasonal and latitude effects on the stratospheric abundance of hydrocarbons. Ref. [18] provided the first one-dimensional (1D) model to incorporate such effects and to track the time- and location-variable influencing the distribution of stratospheric species. This study showed Neptune to have very similar seasonal dynamics to Saturn, while Uranus's were found to be different, primarily due to its 97.8° axial tilt and weak vertical transport. The main hydrocarbons (Table 4) are confined at low altitudes and concentrated at high polar latitudes. The time constants and photochemical lifetimes of these species (except for C_2H_6) were found to be larger than their loss rates, furthering the stratification of hydrocarbons [18]. More recently, a 1D seasonal radiative-convective equilibrium model developed by the Laboratoire de Météorologie Dynamique historically used for Jupiter, Saturn, and exoplanets investigated the origins and evolution of the thermal structure of Uranus and Neptune [85]. This study stressed the importance of knowing the optical properties of haze particles, and changing optical indices will alter the warming or cooling rates in the atmosphere. In addition, a precise CH_4 abundance constraint, with or without haze, will significantly impact the retrieved temperature profiles. Thus, discrepancies between observations and the simulated thermal structure is likely to hint at variations in the latitudinal stratospheric distribution of CH_4 and haze particles [85]. A better characterization of these variables will be crucial to understand the extent of Uranus's thermal impact on the atmospheric composition. A re-analysis of Uranus's energy budget has recently challenged the long-held assumption of a lack of internal heat source [31].

2.4. The Atmosphere of Titan

Titan, the largest moon of Saturn, is uniquely recognized as the sole known natural satellite to possess a dense atmosphere predominantly composed of molecular nitrogen N_2 (∼98%) and methane, CH_4 (∼2%). This reducing atmosphere is stratified into five primary layers—namely, the troposphere, stratosphere, mesosphere, thermosphere, and exosphere (Figure 4)—each exhibiting planetary-scale dynamical, thermal, chemical, and seasonal variations. Temperatures are the coldest (∼70 K) at the tropopause. The formation of the photochemical haze that envelopes Titan is regulated by gas-phase molecular precursors, which are generated in the upper atmosphere through high-altitude N_2 and CH_4 photolysis and radiolysis processes. These precursors consist of hydrocarbon radicals (e.g., CH_2, CH_3), in addition to more complex hydrocarbons, nitriles, and potentially polycyclic aromatic hydrocarbons [86]. Energetic sources facilitating these high-altitude chemical reactions include solar UV photons, solar X-rays, galactic cosmic rays, Saturn's magnetospheric energetic electrons, and the solar wind [87,88]. The Cassini-Huygens mission, over a duration spanning 13 years, conducted an extensive study of Titan, taking direct measurements of the composition in neutrals and ions within Titan's upper atmosphere [86,89]. These investigations elucidated the complexity of Titan's upper atmospheric chemistry, characterized by radicals, neutrals, positive and negative ions, as well as the early stages of solid haze particle formation. On numerous occasions, the measured abundances of specific transient ions such as CH_4^+, $HCNH^+$, $C_2H_5^+$ exceeded predictions from prior models (e.g., [90]). Conversely, the concentrations of certain heavy hydrocarbons and nitrogen-bearing neutral molecules, as determined by the Ion and Neutral Mass Spectrometer (INMS), were found to be lower than anticipated by ion-neutral models ([91], *and references therein*). These findings emphasized the crucial role of magnetospheric electron precipitation and diurnal solar energy variations in modulating molecular distributions within the upper atmosphere.

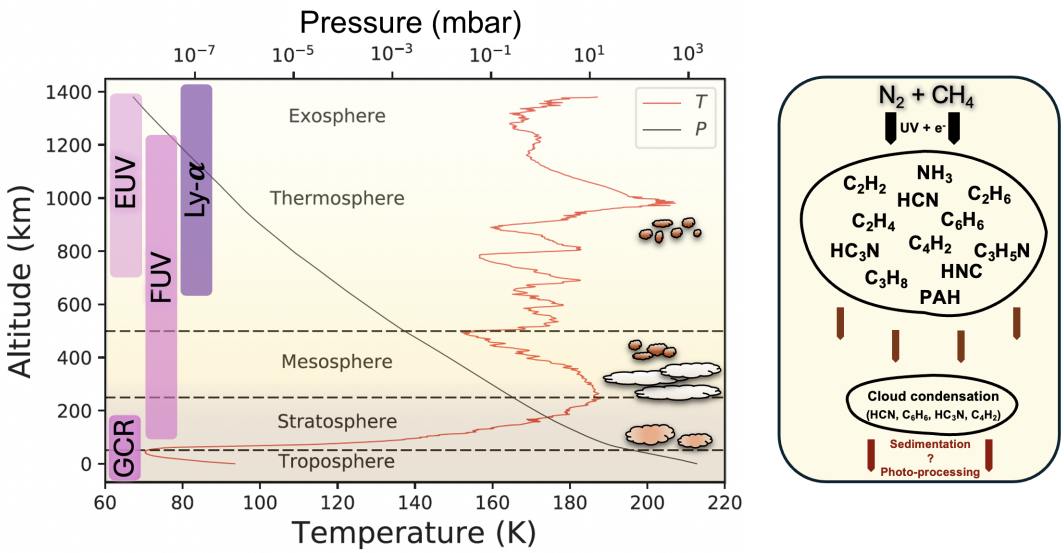

Figure 4. Vertical temperature (red) and pressure (black) measurements conducted by Huygens during its descent down to the surface of Titan. Data obtained from the Planetary Data System: Planetary Atmospheres Node. Adapted from [92].

Connecting Titan's upper atmosphere dynamics with incoming solar and magnetospheric energy deposition started long before Cassini's arrival at Saturn. Benefiting from earlier Voyager 1's flyby of Titan in 1980 [93] at a time when Titan was located inside of Saturn's magnetosphere, it became apparent that Titan was at that time in a moon-solar wind configuration akin to Venus [94]. Well over a decade later, refinements stemming from occultation and plasma experiment measurements led to the expansion of multiple

photochemical models [95–100] along with models incorporating thermal and suprathermal electrons calculations [99]. Based on these measurements, it was found that N_2 EUV airglow emission initiated by photoelectron impact dominated over N_2 airglow triggered by magnetospheric electron impact [99]. Titan's ionosphere operates as a photochemical factory at the interface between incoming solar photon and magnetospheric electron fluxes, and the underlying first steps of molecular and aerosol growth [101].

The solar flux reaching Titan is around 14.8 W m^{-2} (Table 2) and the photon flux at Titan ranges from $\sim 10^6$ ph s^{-1} cm^{-2} nm^{-1} (@60 nm) to 10^7 ph s^{-1} cm^{-2} nm^{-1} (@110 nm) ([102] and Figure 2). As the primary carrier of VUV energy across the solar system (Region 2, Table 1), Ly-α (121.6 nm) has the capacity to penetrate into Titan's upper atmosphere where haze particle formation is initiated. VUV radiation reaches a factor of 100 higher in intensity at 121.6 nm than the baseline at 60–110 nm [102]. Longer wavelength UV photons may even reach lower stratospheric levels which continuously exposes the growing aerosols to the UV radiation ([103] and Figure 4). Modeling of photon and photoelectron deposition on Titan by [103] compared with Cassini Plasma Spectrometer Electron Spectrometer (CAPS/ELS) electron flux measurements at 1014 km showed high matching with the observations. Their comparison confirmed the predominant activating role of photon and photoelectron contribution on the dayside compared to the nightside fluxes derived from the contribution of magnetospheric electrons. The peak photon contribution lies around the ionospheric peak $\sim$1000 km whereas secondary electrons produced from X-rays contribute mostly at lower altitudes (700–900 km). At the latter altitudes and below the tropopause, GRC radiation is estimated to induce $\sim$10 and $\sim$0.1 ionization events cm^{-3} s^{-1}, respectively [104]. At higher altitude, it is estimated that Ly-α photons account for about 75% of all photo-dissociated CH_4 [10,105].

Deeper in the atmosphere, shaped by seasonal dynamics, large polar cloud systems have been observed for over 30 years in Titan's stratosphere. Subject to meridional and vertical transport, these stratospheric clouds have been particularly well-studied in polar winter conditions where they contain several ice spectral signatures (see Section 3) seen in the mid- and far-infrared [106]. Their formation occur at higher altitudes (>168 km) than predicted by models [107] and it is likely that they contain ice co-condensates given their overlapping spectral features [108,109]. An important HCN-rich cloud system was even observed at $z = 300$ km in the south pole after a substantial cooling event in the polar vortex [110,111]. As a result, climate and circulation models have had to be refined and updated after such observations where they could not account for (i) rapid and dramatic changes in the seasonally defined temperature variations, and (ii) shortcomings due to lack of theoretical and experimental aerosol microphysics data [8,111–116]. While these discoveries have helped constrain parameters in General Circulation Models (GCM), they have also left many unanswered questions regarding their ice composition and potential for photochemical evolution [104,108,117–121]. While the intermediate chemical and physical pathways connecting the formation of aerosols and clouds with the gas phase precursors are still not fully resolved, Titan's chemical catalogue remains one of the most complex in the outer solar system.

2.5. Chemical Inventory in Titan

According to the most recent photochemical models, Titan's atmosphere is composed of: hydrogen and hydrocarbons, nitrogenated compounds, oxygenated molecules, and presumed but undetected polycyclic aromatic hydrocarbons (PAH) and reduced phosphorous and sulfur compounds [70,122–127] (See Tables 3 and 4 for summaries of molecules detected, and [10] for an extensive review of Titan's atmospheric composition). The ionization rate peaks around 1150 km. Employing Chapman layer theory, ref. [98] calculated the

peak electron density to occur at 1200 km, [94] at 1175 km, and [128] at 1040 km. The latter study anticipated $HCNH^+$ to be the dominant ion, utilizing a model comprising over 60 species and 600 reactions. Subsequently, Ref. [100] enhanced this analysis, pinpointing the predominant *m/z* 28 peak as $HCNH^+$. Chemical models have helped explain the gas phase chemistry involved in the production of Titan's aerosols (e.g., [70]). Alongside those models, laboratory experiments have helped in vetting the reaction networks through the study of specific channels involving neutral and charged molecular species. Furthermore, photochemical and microphysical models have investigated the dusty nature of Titan's ionosphere (>900 km in the atmosphere) and characterized the interaction between the aerosols and charged particles [129]. More specifically, by using a wide array of energy sources and coupling extensive lists of ion-neutral reactions, models have given insights into the first steps linking small hydrocarbons with larger molecules [70,126,127,130]. Ion-molecule reactions are thought to be directly relevant to aerosol growth, and are controlled by the relative abundances of the two initial neutral main constituents, N_2 and CH_4 [129]. The dissociation of CH_4 by EUV photons results in the formation of methylene $^1CH_2$ in its excited state with a dissociation yield of 0.48 for Ly-α photons, and 0.50 in the FUV (Reaction (1)),

$$CH_4 + h\nu \longrightarrow {}^1CH_2 + H_2 \quad (1)$$

More energetic photons in the EUV (<121.6 nm, Table 1) will preferentially dissociate methane to form the methylene radical $^3CH_2$ in its ground-state (Reaction (2)), while Lyman-α radiation will also form the methyl radical CH_3 with a dissociation yield of 0.42 (Reaction (3), [10]).

$$CH_4 + h\nu \longrightarrow {}^3CH_2 + 2\,H \quad (2)$$

$$CH_4 + h\nu \longrightarrow CH_3 + H \quad (3)$$

The formation of these first radicals in Titan's upper atmosphere by FUV, Ly-α, and EUV photons is a crucial starting point towards the formation of the first intermediate, and then the larger hydrocarbons. Thence begins a long series of cascade of dissociative recombination, proton abstraction, and polymerization reactions that will ultimately lead to the formation of photochemical aerosols (see [70] and Figure 5). The absorption of low-energy (<10 eV) photons as well as much higher energy EUV, by radicals is still poorly understood. Long sought for in the Titan community, CH_3 has perplexed photochemical modeling studies for many years due to its non-direct detection. First, because CH_3 photolysis branching ratios are not well known. Second, CH_3 can be an important source leading to the formation of $^1CH_2$. Third, CH_3 production actually expedites CH_4 loss in Titan's atmosphere, where up to 65% of CH_3 results from CH_4 photolysis with a predicted mole fraction of 10^{-4} at 1000 km, the highest abundance of any of the small radicals in the atmosphere [70]. As a result of this complex radical photochemistry, two hydrocarbons are then produced early on (Figure 5). First, ethylene C_2H_4 forms through the radical-molecule Reaction (4) and then ethane C_2H_6 through the radical-radical Reaction (5) at higher pressure where three-body reactions are permitted, with a peak production at 800 and 200 km [70].

$$CH + CH_4 \longrightarrow C_2H_4 + H \quad (4)$$

$$CH_3 + CH_3 + M \longrightarrow C_2H_6 + M^\star \quad (5)$$

At these altitudes, FUV photons continue to interact with hydrocarbons such as C_2H_2 with low-energy (between 5.5 eV and 12.4 eV) photons which will result in the production of C_2 and C_2H, two radicals involved in significant methane-depletion and hydrocarbon-formation mechanisms [10]. These reactions underscore the contribution of CH_4 photo-degradation by low-energy (<20 eV and especially Ly-α) photons and the

important role radicals play towards the growth of hydrocarbons in a relatively methane-rich environment. This role is particularly important since it also leads to the very molecules that will condense into the lower-altitude clouds and regulate the radiative dynamics of the stratosphere. In recent observations of the late northern summer, CH_3 was detected in the mid-IR by JWST which showed excellent agreement with photochemical modeling abundance results [131], confirming its important role in the neutral atmosphere.

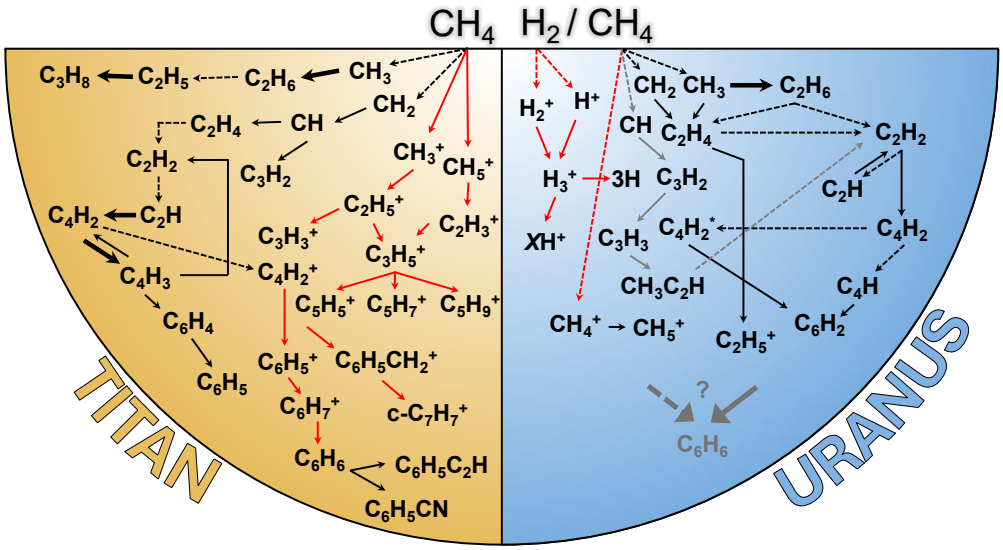

Figure 5. Simplified schematic diagram showing the predominant neutral gas phase hydrocarbon formation pathways in the upper atmospheres of Titan and Uranus, based on available combined observations from Cassini, Voyager 2, Spitzer, IRTF, Hubble, and photochemical models [10,17,21,23,27,34,49,52,70,78,79,95,126,132–145]. Photolysis reactions are shown with dotted arrows, termolecular reactions in thick arrows, and all other types of reactions (neutral, proton abstraction, radical-radical, and radical-molecule reactions) are shown in thin black arrows. Reactions involving ions are shown in red. Note that the reactions in gray leading to the formation of methylacetylene (CH_3C_2H) on Uranus are derived from the photochemical model by [140] developed for the Jovian atmosphere, akin to formation pathways proposed by [146] to explain the as-of-yet undetected C_6H_6 on Neptune.

2.6. From Dynamics to Haze Stratification and Evolution

As outlined above (Section 2.1), atmospheric dynamics play a central role in the transport mechanisms influencing photochemical products, haze formation, and their evolution over time. As such, comparative planetology among all jovian planets and Titan seems necessary to better constrain the underlying mechanisms at play in these cold atmospheres. Irrespective of the planet, constraining each planet's temperature profile is fundamental to derive other atmospheric properties. For example, the refractivity, convection and wind parameters, chemical equilibrium, abundance and condensation of trace gases, cloud formation, precipitation, and particle size distribution are all processes dependent upon or linked to the local temperature gradient. The evolution of haze layers (and the condensation levels of precursor trace gases) is of particular interest since its distribution is shaped by the adiabatic regime and temperature profile [147,148]. With little data regarding this regime and temperature profile on Uranus, it is thus hard to infer any detailed description of the CH_4 (and other condensates) cloud deck stratification and evolution. Moreover, storms and seasonal variations are also likely to affect downdraft and updraft transport, thus modifying a well-stratified cloud condensation structure [148]. Conversely, a poorly mixed stratosphere on Uranus may expose certain haze strata to long-timescale radiative influx, thus potentially affecting their composition. Alternatively, subsiding volatile-rich

air masses resulting from circulation cell reversal on Titan enabled the formation of cloud condensation at higher altitude than expected [111,115]. In parallel, such transport also allows multiple species (C_6H_6, C_4H_2, HCN, etc.) to co-condense, resulting in more complex photochemistry than previously thought. Additionally, a recent re-analysis of solar occultation of Titan prior to the northern spring equinox revealed "leaking" CH_4 from the troposphere into the stratosphere, which reinforces the need for better characterization of the thermal fluxes involved [149]. Furthermore, free parameters such as K_z are poorly constrained and in Titan's stratosphere, K_z values used in photochemical models can vary up to a factor of 100 [126,150]. In summary, both Titan and Uranus provide a unique H_2-rich vs. N_2-rich portrait to investigate their intrinsic dynamical, thermal, and chemical behaviors. Ultimately, improved knowledge of the local temperature and compositional conditions where hazes and clouds form can help guide future theoretical and experimental studies that aim to reproduce the compositional and radiative conditions of Uranus.

3. Photochemistry vs. Radiative Chemistry: Competing Processes and Role in Haze Formation

3.1. Fundamental Processes

Photochemical reactions are fundamental to the plurality of chemical inventories in space since they pertain to electronically excited states and are governed by the law of reciprocity (Bunsen-Roscoe law) in that their reactivity is proportional to the fluence, regardless of exposure time. About nine different types of photochemical reactions relevant to planetary and interstellar conditions exist, and almost twice as many ionizing radiation-based reactions [151–153]. Among these, six of the fundamental reactions are listed hereafter:

- photodissociation: $A^* \longrightarrow B + C$
- quenching: $A^* + B \longrightarrow A + B$
- luminescence: $A^* \longrightarrow A + h\nu$
- photoisomerization: $A^* \longrightarrow B$
- bimolecular reaction: $A^* + B \longrightarrow C + D$
- hydrogen abstraction: $A^* + RH \longrightarrow AH + R$

These reactions occur constantly in planetary atmospheres and serve a fundamental role to initiate gas phase cascade reactions involving radicals and their excited states [10]. Photodissociation reactions primarily contribute to the destruction of CH_4 to form the first radicals (see Section 2), while proton abstraction is thought to be involved in the loss of C_2H_2 to form the first carbon chain anion C_2H^- [10]. Other pathways obtained by [154] applied to the interstellar medium (ISM) have also included bimolecular reactions as an important means of anion growth. Furthermore, infalling H_2O on Titan is expected to participate in the bimolecular reaction with the excited-state $N(^2D)$ atom in the ionosphere [155]. Other reactions such as ion-pair formation or sensitization are also included in photochemical models but their involvement not as well understood [152]. Note that these channels are driven by photons in the NUV to FUV range. In the solar system, and in particular in the outer solar system, low-energy (<10 eV) photons may originate isotropically from (inter)stellar background radiation, particularly the interstellar radiation field (ISRF) and scattered Ly-α in the local interplanetary medium (LIPM) resulting from H_2's excited Lyman and Werner bands, also called the Solomon process. As seen in [18], accurate modeling of these UV sources are required to understand seasonal effects, particularly at the poles of Titan and Uranus where shadowed conditions can last up to several years in the winter hemispheres. These regions can thus be more favorable to rapid CH_4 photolysis with its dissociation energy threshold of 4.52 eV (Figure 2). Likewise, with a low-energy dissociation threshold of 4.48 eV, H_2, a symmetrical molecule, presents

only one vibrational mode as its indirect dissociation occurs through the continuum of the ground electronic state. Notwithstanding limiting cold temperatures, heterogenous chemistry may also come into play where solid grains or polycyclic aromatic hydrocarbons (PAH) may catalyze H_2 formation through chemisorption or physisorption, a process well-studied in photodissociation and other PAH-enriched regions [156].

In addition, radiation chemistry includes pathways pertaining to processes resulting from the interaction between the gas or condensed phases and ionizing radiation above the ionization threshold ~10 eV. A unique feature emanating from radiation chemistry is the generation of a cascade of low-energy secondary electrons [157–160]. These electrons's energy have been shown to induce substantial chemical changes on cosmic ice grains, and have even been proposed to participate in the formation of certain prebiotic molecules [161,162]. In [159], the authors studied radiolytic mechanisms of degraded NH_3 ices in ISM-like conditions, bombarded with ~1 keV electrons accompanied by low-energy electrons (~7 eV). The authors found that non-ionizing radiation of condensed NH_3 (ammonia expected to be the most abundant nitrogen-bearing compound in the ISM, while also present in the gas phase formed in Titan's ionosphere, and in the condensed state in Uranus's troposphere, Figure 3) was responsible for the formation of hydrazine (N_2H_4) and diazene (N_2H_2) in the condensed phase. It was proposed that a first step involved the dimerization of the NH_2 radical due to >1 keV impact, followed by a favorably energetic dissociative electron attachment (DEA) at 6 and 10 eV [159]. As surveyed in [153], low-energy secondary electrons generated by radiation chemistry can lead to reaction pathways that are otherwise not relevant to photochemistry. Unlike photons, electrons can induce singlet-to-triplet transitions via exchange interactions with electrons [158]. Additionally, electrons can be transiently captured by molecules, forming temporary negative ions (TNIs) through resonant processes such as shape and core-excited resonances [163,164]. These TNIs may undergo dissociative electron attachment (DEA), leading to bond cleavage and the generation of reactive fragments capable of further chemical transformations [153,165]. Through the combination of the yield of secondary low-energy electrons generated by radiation chemistry with UV photons dissociating and exciting molecules, these competing processes contribute to diversifying the molecular inventory necessary for the rapid molecular growth leading to the formation of aerosols in planetary atmospheres. The following reaction mechanisms are only a handful [166,167].

- Ionization: $AB \longrightarrow AB^+ + e^-$
- Ion dissociation: $AB^+ \longrightarrow A^+ + B$
- Ion-molecule reaction: $AB^+ + BC \longrightarrow$ Products
- Electron attachment: $e^- + M \longrightarrow$ Products
- Fluorescence: $AB^* \longrightarrow AB + h\nu$
- Excimer formation: $A^* + A \longrightarrow A_2{}^*$

Another process still poorly understood concerns multiphoton and fluorescence chemistry, which was first observed by [168], resulting from the photodissociation of simple hydrocarbons such as C_2H_2 and C_2H_4. In that study, UV photon (193 nm) absorption alone was not able to explain the fluorescence of free radical photo-products. To account for this discrepancy, the authors put forth the proposition of a sequential absorption scheme where molecule AB* absorbs a secondary photon, a concept revisited in [169] to understand cometary emission of C_2. Relevant to Uranus's lower atmosphere, the multiphoton ionization of H_2S [170–172] or even PAHs (e.g., [173]) have been studied in order to understand the ionic fragmentation patterns involved in the UV-VIS region. The processes involved in radical photochemistry and secondary photolysis still remain to be characterized in the context of planetary atmospheric chemistry (Table 5).

Table 5. Comparative general characteristics of photochemistry and radiation-induced chemistry in atmospheric and astrochemical processes.

Characteristics	Photochemistry	Radiation-Induced Chemistry	Examples
Energy source	Ly-α; UV continuum	EUV/X-rays; energetic particles	100–400 nm; secondary electrons; ions
Primary effect	Photodissociation; photoionization; electronic excitation	Ionization; radiolysis; dissociative electron attachment	$CH_4 + h\nu \rightarrow CH_3 + H \rightarrow H^- + CH_3^+$
Key products	Radicals; small hydrocarbons	Ions (e.g., CH_3^+); complex organics; electrons	H_2^+, CH_3, CH_3^+, $C_2H_3^+$, $C_3H_4^+$
Timescales	ns–hours (daylight-driven)	fs–ns (instantaneous, flux-dependent)	$H_2O \rightarrow H\bullet + OH\bullet$ (spur reactions)
Temperature dependence	Strong (Arrhenius kinetics)	Weak (governed by particle flux)	$CH_4 + H \rightarrow CH_3 + H_2$
Electron transfer	Charge transfer	Ionization cascades; secondary electron emission	$O^+ + CH_4$
Quantum effects	Electronic transitions; spin-forbidden pathways	Ro-vibrational excitation; plasmon resonances (ices)	singlet-triplet absorption
Observables	Dayglow emissions; gas abundances	Auroral X-rays; Lyman-Werner band emissions; mass spectra of ices	mass spectra, IR-UV spectra
Altitude/region	Stratosphere; ionosphere (day side)	Thermosphere; polar auroral zones; interstellar ices	$NH_3 + h\nu \rightarrow NH_2 + H$
Desorption yields	Low–moderate (UV-photon dependent)	High (sputtering by >100 eV electrons)	$CO + e^- \rightarrow CO_{(ads)} \rightarrow CO(g)$
Multiphoton effects	Rare	Dominant (ionization cascades; track formation)	$CH_4 \rightarrow CH_3^+ + e^-$ (15.6 eV)

References: [152,153,159,174–178].

Pathways involving ions are too numerous to include here and the reader is referred to [10,18,70] for an updated in-depth overview of known reaction schemes for Titan and Uranus. Instead, a focus hereafter will be placed on the competition between photochemical vs. radiative processes (impacting excited and dissociative ion chemistry, respectively) since ion reactivity remains a crucial component to investigate to understand haze formation in the solar system, interplanetary, and interstellar ices [152,153,160,166]. Numerous studies have investigated the photochemical effects induced by Ly-α on interstellar matter which represents a good benchmark for heterogeneous chemistry conducive to the formation of organic molecules in the solar system [160,161,167,179,180]. Furthermore, FUV, EUV, and even NUV radiation has been shown to induce chemistry in the condensed state in laboratory Titan ice and aerosol analogues [104,119–121,178]. In Titan's upper atmosphere, photochemically produced haze will indeed interact with these UV photons, thus modifying their composition and the ice CCN down to mesospheric and stratospheric altitudes. The extent of this $h\nu$-induced chemistry remains far from being fully characterized, and the task becomes even worse for Uranus. Here, we will present a summary of studies that have probed Titan's and/or Uranus's photochemical processes vs. those that have investigated radiation chemistry at energies $<$ 50 eV utilizing (primus) Cassini/Voyager

or ground-based observations, (secundus) experimental analyses simulating Titan-like low-temperature reactivity in the condensed state initiated by low-energy (<20 eV) photons and electrons, (tertius) advances in the theoretical study of branching ratios and their relevance in the VUV, and (quartus) considerations of the relatively poorly understood role of dication species and their reactivity through vertical ionization processes.

3.2. Observational Considerations: From Low-Mass to Intermediate-Mass Molecules

3.2.1. Low-Mass Species

As part of this discussion and the species discussed below, we will follow the simplified classification from [181,182] separating low Z and high Z elements found in Jovian planets, resulting from photochemistry and radiation chemistry processes. Low Z elements revolve around H and He, while high Z elements concern any species with a mass higher than He. A focus will be placed primarily on the role of H on Titan and Uranus, and H_3^+ on Uranus. About 20 years separate the first detection of H_2 on Uranus [47] and on Titan [183]. Two decades later, H_3^+ was detected on Uranus, serving as an important temperature proxy in the upper atmosphere from its emission intensity-dependence on solar activity [139,184]. Figure 6 shows the observed spectrum of H_3^+ and the intense $Q(3)$ band centered at 3.985 μm with the open source model fit using the `h3ppy` package (version 0.6.1). The chemistry of H_3^+ on Uranus mainly involves daytime and nighttime processes. EUV photons (>10 eV) on the dayside of Uranus ionize H_2 which produces H_2^+ and a free electron (Reaction (6)). H_2^+ then reacts with the background H_2 to produce H_3^+ through the exothermic Reaction (7). Recently, other channels have been proposed to explain H_3^+ formation, requiring impact ionization of C_2H_6 by higher energy electrons (300 eV) [185] and from doubly ionized cyclopropane C_3H_6 [186]. The atomic yield of hydrogen through these channels is an important consideration since, as pointed out in [79], (i) H loss by chemistry (Reactions (8) and (9)) influences the recycling and abundance of CH_4, and (ii) controls the production of polyacetylenes such as C_4H_2 from competing quenching of metastable excited $C_4H_2^{**}$ by H_2 and bimolecular reaction pathways. Note that H_3^+ was recently detected for the first time at Neptune with JWST [187].

$$H_2 + h\nu \longrightarrow H_2^+ + e^- \quad (6)$$

$$H_2^+ + H_2 \longrightarrow H_3^+ + H \quad (7)$$

$$H + C_4H_2 + M \longrightarrow C_4H_3 + M \quad (8)$$

$$H + C_4H_3 \longrightarrow C_4H_2 + H_2 \quad (9)$$

C_4H_2 being a strong absorbent of UV light, it is likely to be excited into the metastable state $C_4H_2^{**}$ between 180 and 260 nm, a process more likely to occur on Uranus than in the nitrogen-rich atmosphere of Titan [79]. These reactions were later taken into account in [138], and the later detection of C_4H_2 by [52] raises the question of what the extent of these small hydrocarbons on Uranus is and the competing roles between photochemistry, radiation chemistry, and condensation processes which might affect the abundances of polyacetylenes in the atmosphere. Furthermore, as shown in stratospheric photochemical modeling [18], the latitudinal distribution of hydrocarbons is strongly dependent on seasonal effects (i.e., solar radiation), and thus on photochemical efficiency. On Titan, the chemistry of low Z elements is relatively less influential than that on Uranus, since H_2 concentrations on Titan are much lower (∼0.4% [188]). Still, atomic hydrogen is thought to originate mainly from CH_4 photolysis (other subsurface sources may also exist [189]), although its exact vertical profile and source/sink equilibrium are still debated ([10], *and references therein*).

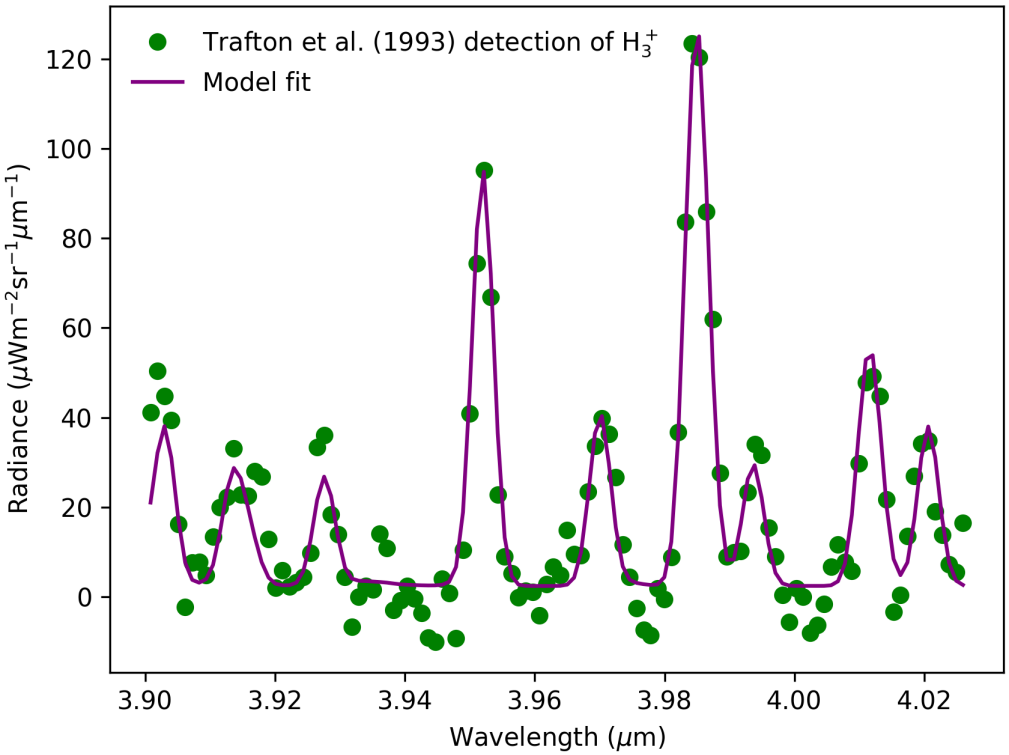

Figure 6. Observed spectrum of H_3^+ (green dots) detected by [139] between 3.89 and 4.03 µm, a range which includes the region with multiple lines of the *Q* branch of H_3^+, with the most intense *Q*(3) band at 3.985 µm [143]. A model fit using the `h3ppy` open source package computed with a rotational temp 740 K is shown in purple. Here, the model retrieves an H_3^+ column density of 4.42×10^{14} m^2 (https://github.com/henrikmelin/h3ppy, accessed on 21 May 2025).

3.2.2. Higher-Mass Species

Higher Z-mass species ($m/z >$ He) between Titan and Uranus share one common chemical entry point: the photo-destruction of CH_4 (Figure 5). As discussed above, C_4H_2 with a mass of 50 amu remains the highest mass of a molecule detected on Uranus, while negatively charged particles with masses of over >10,000 amu are the largest detected on Titan (albeit with no exact molecular identification to date). If, on Uranus, intermediate mass molecules (C_2H_2, C_2H_6, C_4H_2) do condense out near their production altitude [138], UV-driven solid-state chemistry becomes a possibility, although this is at present a field almost completely unexplored. As pointed out in [142], photolytic destruction branching ratios of C_2H_2 and formation kinetics of C_2H_6 from $^1CH_2$ are also not well constrained and model-sensitive, which can result in significant modeled abundance variations. The formation of PAHs is also an unresolved question, as they have only been indirectly identified on Titan [190], while C_6H_6 alone has so far not been detected on Uranus. Recent experimental work in this field has shown promising results (see Section 3.3). In order to broaden our understanding of Uranus's molecular distributions, it may be advantageous to focus future research efforts on the reactivity of C_2H_2 with other primary hydrocarbons. Improving our understanding of the chemistry of this compound, a precursor to polyynes, cyanopolyynes, and potentially PAHs, may facilitate the future detection of novel species [144].

As seen in Section 2.4 and Figure 5, the net end result of CH_4 photolysis due to UV photons results in high Z hydrocarbons (Table 4). With Titan and Uranus having reducing atmospheres, high-altitude haze formation benefits from the supply of EUV radiation which in turn heats the haze layers and creates the observed high-altitude temperature inversions (see Figure 4). These mechanisms have been well characterized on Titan and remain poorly known on Uranus [63]. In spite of the tropopause cold-trap, condensing

species such as CH_4 manage to rise into the stratosphere under unknown mechanisms [20], possibly due to moist convection. This transport brings CH_4 to higher altitudes (an effect even more pronounced on Neptune due to stronger mixing) whereby VUV photons begin photodissociation and photoionization [20]. The most abundant photolytic product, C_2H_6 is important on Titan for several reasons. First, it is one of the first photochemically produced hydrocarbons and reaches $\sim 10^{-6}$ in the stratosphere (Table 4) with detections of ice spectral signatures thought to correspond to ethane ice condensation above the tropopause over the north pole [191,192]. Second, its formation involves ion-neutral reaction coupling associated with methane loss via Reaction (5). Also, once formed, neutral ethane is likely to react with C2 cations resulting in the formation of C3 and C4 ions [70], thus accelerating molecular growth. In the EUV/FUV wavelength range, C_2H_6 destruction mainly leads to the formation of ethylene C_2H_4 and two hydrogen atoms, while at longer wavelengths (>140 nm) C_2H_4 is formed along with H_2, with branching ratios of 0.30 and 0.12, respectively (see Section 3.5). This is an important step since not only is ethane an important intermediate in the photochemical production of atomic and molecular hydrogen on Titan (although the majority of hydrogen is formed thanks to CH_4 photolysis), but also because DEA of H_2 may thus form the H^- anion where low-energy (4 eV) trapped electrons reside in a resonant state within H_2 [193]. Molecular hydrogen is also efficiently produced through the photodissociation of ethylene C_2H_4 with UV photons between 118 and 175 nm [194,195] through the following reaction pathway:

$$C_2H_4 + h\nu \longrightarrow C_2H_2 + H_2 \quad (10)$$

This constitutes an important reaction since (i) ethylene (first discovered by [196]) is the smallest alkene (i.e., the two C atoms are linked by a double bond) and the only photochemical hydrocarbon to never condense at Titan's tropopause, and (ii) photolysis of C_2H_4 incorporates a $\pi \rightarrow \pi^*$ excitation where absorbed low-energy photons (<10 eV) lead to an electronically excited state of the molecule. In this excited state, ethylene may go through photoisomerization or proton abstraction reactions, Furthermore, ion-neutral reactions play here a key role for molecular growth by producing some of the first C3 (Reaction (11)) and then C5 (Reaction (12)) ions, what has been described by [10] as a "stepping stone from methane to higher hydrocarbons". The reactivity of C_2H_4 with $N(^2D)$, the first electronically excited state of atomic nitrogen produced by VUV photons, has been studied on Titan and plays a key role in the loss of $N(^2D)$ as well as the formation of nitrogenated products [197]. Overall, photochemistry is thus a fundamental mechanism to rapidly convert small molecules into larger organics.

$$C_2H_4 + {C_2H_5}^+ \longrightarrow CH_4 + {C_3H_5}^+ \quad (11)$$

$$C_2H_4 + {C_3H_5}^+ \longrightarrow H_2 + {C_5H_7}^+ \quad (12)$$

3.2.3. Polycyclic Aromatic Hydrocarbons: Agents of Haze Growth?

On Titan, the composition of gas phase products with masses > 78 amu, corresponding to C_6H_6, is still largely unknown. Data in this molecular mass regime (heavy ions and neutrals) is austere and can be summarized in three broad categories, though with no exact molecular formulae. First, aliphatic compounds that comprise C_2H_2 polymers, nitrogenated polymers, and aliphatic copolymers [89]. These broad mass groups (possibly up to C14) have only been detected in their positively charged form by Cassini, at altitudes where EUV radiation peaks in the ionosphere (~1000 km). Second, PAHs and nitrogenated-PAHs have been tentatively detected, with naphthalene (${C_{10}H_8}^+$) and anthracene (${C_{14}H_{10}}^+$) being candidate cations [89,156]. Ion-neutral pathways are likely dominant processes for their

formation. In the gas phase, VUV photons are generally needed to ionize PAHs through radiation chemistry. Recently, Ref. [198] investigated the low-temperature visible-light photoionization of PAHs trapped in crystalline ice. The authors found that trapped PAHs in low-temperature water ice had their ionization threshold lowered by 4.4 eV with respect to their neutral gas phase counterparts. This opens new venues towards the characterization of potential PAHs in the atmospheres of Titan and Uranus. Third, negatively charged compounds (anions) have long remained a core question related to the gas composition of the upper atmosphere of Titan since their discovery by [199]. More details on them are given in Section 4.

To date, neither benzene or PAHs have not been detected on Uranus (or Neptune). However, a point should be made here to address the photochemistry of C_6H_6 and PAHs of relevance to Uranus, through comparative planetology with Jupiter and Saturn. A search for C_6H_6 was conducted on all gas giants by [200] using the Infrared Space Observatory. While abundance values were determined for Jupiter and Saturn, only upper limits were provided for Uranus and Neptune. Early photochemical modeling by [140] containing only neutral-neutral reactions and Ly-α radiation originating from the LIPM did not predict the formation of C_6H_6 on the two ice giants, and acknowledged the need for accurate C_6H_6 absorption cross-sections, branching ratios at low temperature and low pressures. Loss mechanisms part of their model included C_6H_6 destruction by photolysis to form either a phenyl group (C_6H_5) or C_6H_4. Another important assumption, based on Jovian photochemistry, was that C_6H_6 in an excited "hot" state stabilizes through collisions once transported down to Jupiter's lower stratosphere [140], although the authors also note the possibility for benzene to be produced by ion-neutral reactions in aurorae-rich regions. Putative stabilization of benzene may thus prevent the molecule from dissociating [140]. The non-detection of benzene on Uranus (or Neptune), however, has renewed interest in incorporating ion chemistry to models, particularly when using Titan as a baseline [142,146]. In [146], coupling ion-neutral pathways brought predicted mole fractions of benzene from $\sim 10^{-13}$ (neutral reactions only) to $\sim 10^{-9}$–10^{-10} (ion-neutral reactions) between 1 µbar and 1 mbar in Neptune's stratosphere. We can expect there to be similar reactions occurring in Uranus's atmosphere, although important caveat variables exist such as (i) temperature-dependent photodissocative branching ratios, (ii) electron dissociation recombination rates, (iii) cloud microphysics and equilibrium vapor pressure measurements at low temperature, and (iv) vertical transport [115,146,201]. Furthermore, photochemical reaction pathways, either omitted from models or whose branching ratios are unknown, involving C_2H_2 or its derivatives, remain to be explored [144]. As pointed out in [202], laboratory measurements of electron recombination rates of $C_6H_7^+$ by low-energy electrons (<1 eV, Reaction (13)) with a rate constant of ($\alpha = 2.4 \times 10^{-6}$ cm^3 s^{-1} valid for electrons temperatures between 300 and 800 K) and their products are key yet unknown parameters needed to understand the formation pathways leading to benzene. Other pathways such as the trimerization Reaction (14) may also be relevant to surface or tropospheric conditions on Titan due to GCR radiation [144]. Once C_6H_6 is formed, PAH formation may also be possible through the ethynyl addition mechanism (Reaction (15)) for which both Titan and Uranus may provide suitable low-temperature, hydrogen-rich environments [144,203].

$$C_6H_7^+ + e^- \longrightarrow C_6H_6 + H \quad (13)$$

$$3\,C_2H_2 + GCR \longrightarrow C_6H_6 \quad (14)$$

$$C_6H_6 + C_2H \longrightarrow C_6H_5C_2H + H \quad (15)$$

Finally, catalytic reactions on the surface of interplanetary grains with the interaction of C_2H_2 with SiC has been shown to be an efficient mechanism to produce cyclic and/or

prebiotic molecules (see [144] for a detailed review on the matter). Delivery of SiC grains (found in meteorites and comets) and subsequent chemistry with C_2H_2 may lead to C_6H_6 formation, while silicon dicarbide c-SiC_2 (found in the ISM) may be produced by the UV photolysis of c-SiC_2H_2 (Reaction (16), [144,204]). The kinetics of these reactions, and thus their capacity to act as efficient catalyzers for larger organics formation, remains an open field of study, one of interest for the cold outer solar system. More recently, quantum chemistry calculations explored gas phase cyanobenzene formation routes catalyzed by the NCN^- anion [205].

$$\text{c-}SiC_2H_2 + h\nu \longrightarrow \text{c-}SiC_2 + H_2 \quad (16)$$

3.3. Laboratory Experiments: Simulating Atmospheric Chemistry

From the first seminal set of studies designed to mimick the UV- and magnetospheric-field of radiation of an outer solar system body (Titan), laboratory experiments have unveiled many processes involved in the formation of laboratory analogues of planetary aerosols called *tholins* [7,8]. These studies have used multiple sources of energy to simulate either the UV photon radiation reaching the upper atmosphere of Titan, or more energetic Ly-α or GCR radiation. In the former case, electrical plasma discharges have been widely used as a realistic analogue of solar radiation-induced chemistry as impact from inelastic electron collisions will dissociate the carrier gases CH_4 and N_2, and their overall electron energy distribution functions resembles that of the solar spectrum [102]. The electrons deposited on N_2-based gas mixtures thus lose their energy through inelastic collisions and are able to initiate the chemistry between N_2, CH_4, and any other gas present in the mixture. To reproduce the more intense radiation such as Ly-α photons, GCRs, or higher-energy photons, dedicated microwave plasma sources or synchrotron facilities (for energies < 200 nm) have been utilized. A panorama of these facilities used to simulate Titan's atmospheric chemistry, from those studying gas phase to condensed-phase chemistry, is shown in Table 6. The reader is referred to [7] for a historical overview of experimental simulations of *tholin* formation to simulate Titan's atmosphere.

Table 6. Panorama of past and current experimental facilities enabling the chemical study in the laboratory of simulating various typical energy sources reaching Titan's atmosphere. The broad objectives for each experimental setup are also annotated. SE correspond to low-energy secondary electrons.

Category [1]	Main Processes	Energy Source	References
Gas phase	Ionization, dissociation, radical chemistry	Plasma discharges	[206–226]
	Photolysis, radical, excitation, SE	FUV–Ly-α–EUV	[220,227–240]
Tholins/ice	Condensation, solid-state photochemistry, SE	FUV/VUV	[104,119–121,178,198,241–247]
Synchrotron	Ionization, dissociation, excitation, SE	EUV-VUV Target wavelength	[232,233,236,248–251]

[1] Note: experimental needs for Uranus using similar techniques are listed below.

Currently, laboratory simulations of Uranus's atmosphere are severely limited. As discussed previously, multiple parameters needed to better understand our comprehension of photochemical haze formation under low-energy (<50 eV) particles are lacking from state-of-the-art photochemical models. Such parameters and uncertainties can be corroborated by experimental simulations using analogous Titan techniques as a basis to probe the chemistry in H_2-based environments. Laboratory experiments such as those listed in Table 6 are in an opportune time to address these knowledge gaps, whether in determining

accurate reaction kinetics, branching ratios, or in studying the photochemical evolution of organic and sulfuric Uranus-relevant ices. Following the themes outlined in [20,63], more details and future perspectives are given below and in Section 5.

- *Atmospheric chemistry science:* Multiple complementary laboratory experiments (Table 6) utilizing different sources of energy (plasmas, UV lamps, high-energy synchrotron beamlines) are substantial to probe specific chemical and photoionizing processes. In particular, questions surrounding the role of ion-molecule chemistry and haze growth on Titan have significantly benefitted from laboratory studies. Coupled with in situ or ex situ analyses such as high-resolution mass spectrometry, IR spectroscopy, electron microscopy, secondary ion mass spectrometry, X-ray photoemission spectroscopy, atmospheric-pressure photoionization, just to name a few, future measurements would provide much insights into the chemical composition of Uranian *tholins* and gas phase precursors. Furthermore, laboratory characterizations of photochemical products would help support in situ measurements by a future UOP and help quantify these precursors resulting from the photodissociation of CH_4, NH_3, etc.
- *Cloud science:* Laboratory measurements of the physical and optical properties of any Uranian laboratory-produced aerosols would directly provide valuable information to interpret cloud observations and the modeled scattering, nucleating, and size properties of the CCN. Their properties would then help address the role and interaction of clouds with condensable species. Moreover, studies of the photochemical evolution under low-energy (as well as of much higher-energy) photon irradiation remains critically unexplored.
- *Chemical kinetics & thermodynamics:* As outlined below, kinetic rates, branching ratios, and absorption cross-sections are fundamental properties that are needed to solve model degeneracies and inaccurate abundance retrievals (Table 7). Future theoretical calculations combined with experimental measurements are much needed.

3.4. Condensed Phase

Ice cloud spectral signatures have been detected on both Titan and Uranus (see Section 2). The clouds in these atmospheres are tropospheric/stratospheric and can be at similar altitudes to the photochemical hazes [8,21,252]. Over more than a decade, multiple studies have investigated the low-temperature reactivity of Titan ice cloud analogues under UV photon irradiation. These studies have also measurement the fundamental properties of these Titan-relevant ices/*tholins* with no energy input, e.g., IR absorption spectroscopic [109,252] and their optical properties [253], and vapor pressures [115,254], as well as UV photon and synchrotron light irradiation (see Table 6). Reproducing stratospheric ice photochemistry has had to adapt to the ever-evolving knowledge of Titan's stratospheric composition and seasonal variations. Nonetheless, ice mixtures have typically been formed from any of the following molecules CH_4, C_2H_2, C_4H_2, C_6H_6, HCN (Table 6). The overall objective of these studies can be summarized in two broad categories: (i) reproducing spectral features seen by Cassini's Composite Infrared Spectrometer (CIRS) in the mid- and far-IR, and (ii) measuring the spectroscopic and chemical impacts of FUV photon irradiation on these ices. In the latter case, few laboratory apparatus have explored the ageing of UV-induced photochemistry. The Physique des Interactions Ioniques et Moléculaires (PIIM) laboratory at Aix-Marseille Université has been conducting studies of the photochemical evolution of Titan-relevant organic ices for over a decade. The foundational work for these measurements was established through the VUV-induced photosynthesis of organic molecules trapped in solid argon matrices at low temperatures [255,256]. In [256], the authors used a microwave-driven hydrogen lamp which generated FUV photons with energies 3–10 eV and generating a photon fluence of $\sim 10^{15}$ photons cm^2 s^{-1} to irradiate

the Ar matrix doped with a C_2H_2:HC_5N mixture. The induced photochemistry resulted in the production of HC_7N and further confirmed the possibility to generate long condensed state carbon-nitrogen chains trapped in solid Ar. Since, experiments to simulate the photochemical processing of Titan-relevant molecules at cryogenic temperatures has included C_2H_2 [244], C_6H_6 [121,246,247,257], C_4N_2 [104], HCN, HC_3N, and HC_5N [119,120], and ethyl cyanide CH_3CH_2CN pure ice [243]. Note in the latter case, higher energy photons (>120 nm) were used and yielded several organics such as ethyl isocyanide CH_3CH_2NC, vinyl cyanide CH_2CHCN, and hydrogen cyanide HCN. Such studies not only highlight the potential for low-energy photons to initiate solid-state chemistry in lower atmospheric regions where high-energy photons are rare, but also because they may help in retrieving desorption energies, photodissociation cross-sections, or the branching ratios of products resulting from UV photolysis [243]. In [178], FUV photons at >300 nm were found to initiate condensed-state photochemistry in C_4N_2 ices through singlet-triplet excitations (population of triplet states only) whereas at shorter wavelengths (266 nm) kinetics are faster due to singlet-singlet excitation processes [104,178]. Photon fluxes in these laboratory experiments reach $\sim 10^{17}$ photons cm^2 s^{-1} which corresponds approximately to <10 Earth years on Titan depending on the experimental irradiation integration time [178]. In addition, with much higher fluxes, synchrotron light is an extremely useful tool to explore a much wider range of energies; these studies are summarized in Table 6.

Several of the molecules mentioned hitherto posses their first excited singlet ($S_0 - S_1$) or triplet ($S_0 - T_1$) state thresholds in the FUV-VIS region which makes them particularly relevant study under cryogenic conditions, and relevant to the cold planetary atmospheres of the outer solar system [119]. As a result, solid-state photochemistry is permitted to occur at longer wavelengths than in the gas phase by reducing the excitation energy threshold of new electronic states. In these conditions, photochemistry initiated by low-energy (<20 eV) photons at altitudes where organic ice clouds form is plausible and may lead to pathways where ice CCN may harbor more advanced prebiotic chemistry [178]. These processes have been extensively studied in environments applicable to the ISM ([160], *and references therein*). Other ice mixtures containing more species of the CHNOPS family may for future laboratory work be relevant to incorporate and to investigate the photon- and electron-induced chemistry. For example, the radiolysis of ammonia (NH_3) under low-energy (7 eV) electron impact resulted in the production of the nitrogen-rich hydrazine (N_2H_4) and diazene (N_2H_2) [159]. In their work, incident electrons with energies as low as 6 eV permitted excition processes leading to the production of NH_2 radicals at 20 K while also producing the hydride anion H^-. In parallel to photodissociation mechanisms, electronic excitation was shown to be a crucial process in the electro-processing of NH_3 ice. While ammonia remains to be directly detected on Uranus (and importantly, as it condenses to form ammonium hydrosulfide NH_4SH clouds, see Figure 3), its stratospheric and tropospheric photochemical evolution (along with the other CH_4 and H_2S clouds) persists as a mystery.

Table 7. Selected branching ratios (*br*) of photodissociation at Ly-α (121.6 nm) wavelengths (or in ranges including Ly-α as indicated if necessary) for CH_4, H_2, C_2H_2, C_2H_4, C_2H_6, CH_3C_2H, C_3H_8, C_4H_2, CH_3CN, and H_2S. AROM indicates a summed list of 14 neutral aromatics.

Molecule	Photochemical Products	*br*
CH_4	$CH_3 + H$	0.42
	$^1CH_2 + H_2$	0.48
	$^3CH_2 + 2H$	<0.1
	$CH + H_2 + H$ or $C + 2H_2$	<0.1

Table 7. *Cont.*

Molecule	Photochemical Products	*br*
H_2	$H_2^* \rightarrow H_2 + h\nu'$ (fluorescence) H + H (predissociation)	0.8–0.9 0.1–0.2
C_2H_2	$C_2H + H$ $C_2 + H_2$ $C_2H_2^* \longrightarrow C_2H_2$ $C_2H_2^+ + e^-$	0.3 0.1 0.6 0.84 [a]
C_2H_4	$C_2H_2 + H_2$ $C_2H_2 + 2H$	0.58 [b] 0.42 [b]
C_2H_6	$C_2H_4 + H_2$ $C_2H_4 + 2H$ $C_2H_2 \longrightarrow 2H_2$ $CH_4 + {}^1CH_2$ $2CH_3$	0.12 0.30 0.25 0.25 0.08
CH_3C_2H	$C_3H_3 + H$ $C_3H_2 + H_2$	0.56 [c] 0.44 [c]
C_3H_8	$C_3H_6 + H_2$ $C_2H_6 + {}^1CH_2$ $C_2H_5 + CH_3$ $C_2H_4 + CH_4$	0.34 [d] 0.09 [d] 0.35 [d] 0.22 [d]
C_4H_2	$C_4H + H$ $2C_2H$ $C_2H_2 + C_2$ $C_4H_2^*$	0.20 [e] 0.03 [e] 0.10 [e] 0.67 [e]
CH_3CN	$CH_3 + CN$ $CH_2CN + H$	0.20 [f] 0.80 [f]
H_2S	$H_2 + S(^1D)$	<0.12 [g]
AROM	C_6H_6 + photoproducts	0.1–0.3 [h]

[a] From 166 to 190 nm. [b] From 118 to 175 nm. [c] Extends up to 220 nm. [d] From 115 to 135 nm. [e] From 120 to 164 nm. [f] Below 235 nm. [g] For $\lambda = 139.11$ nm. [h] Model estimates from [142]. Note: Although propane C_3H_8 has not been detected on Uranus, it has been proposed in some photochemical models. References: [122,142,180,194,258–264].

3.5. Branching Ratios

UV wavelength-dependent branching ratios are one of the fundamental components required to accurately simulate photochemical pathways relevant to planetary atmospheres [194]. With the modern advances in quantum-chemistry calculations, these important tools can provide accurate quantum yields and branching ratios for the photodissociation of neutral molecules (see Table 7), positive ions (Table 8), and even of vibrationally excited states of hydrocarbons of relevance [265]. Although non-exhaustive, the tables below provide wavelength-dependent branching ratios for some simple hydrocarbon photolysis reactions that have been included in Titan, Uranus (and Neptune) photochemical models.

Table 8. Selected quantum yields of ion-neutral and neutral-neutral reactions relevant to Titan and Uranus.

Reaction	Photochemical Pathway	Quantum Yield (Φ)
$N^+ + CH_4$	$CH_3^+ + NH$	0.50
	$CH_4^+ + N$	0.05
	$H_2CN^+ + H_2$	0.10
	HCN+ + NH + H	0.36
$N_2^+ + CH_4$	$CH_2^+ + N + H_2$	0.09
	$CH_3^+ + N + H$	0.91
	$N_2H^+ + CH_3$	-
$CH_3N_2^+$	$N_2CH_2^+ + H$	0.01
Atom	**H production channels**	**H atom yield**
H	$CH + CH_4$	1.00
	$CH + C_2H_6$	0.22
	$CH + C_2H_6$	0.14
	$CH + C_3H_8$	0.19
	$CH + C_4H_{10}$	0.14

References: [140,240,258–260,266,267]

3.6. Dication Chemistry and Photo Double Ionization Processes

Fragmentation processes in the gas phase with respect to divalent states have recently, when investigating ionization chemistry mechanisms, gained interest. Indeed, double photoionization and photoelectron impact calculations of N_2 for the first time by [268] in Titan's upper atmosphere predicted an N_2^{++} layer located at the ionospheric peak (∼1150 km, Reaction (17)). Fluorescence may even be observed for N_2^{++} [268].

$$A + h\nu \longrightarrow A^{++} + 2\,e^- \tag{17}$$

The double photoionization thresholds for our atoms and molecules of interests (i.e., C, N, abd N_2) all occur at energies < 45 eV (34.4 eV for CH_4; the reader is referred to the detailed review by [269], Table 1, on doubly charged ions in planetary atmospheres). Recently, vertical ionization pathways of bimolecular $[CH_4–N_2]^{2+}$ or $[CH_4\cdots CH_4]^{2+}$ clusters have been calculated and provided key insights into the role of monovalent and divalent states of simple hydrocarbons may play in planetary environments [185,269–271]. In [270], ionized fragmentation processes led to monovalent $[H_3C–HN_2]^+$ and divalent $[H_4C–N_2]^{2+}$ intermediates with no energy barrier. This is an important characteristic since in its "ionized growth", a bimolecular cluster may thus produce a stabilized intermediate having acquired enough excess energy, making it possible to overcome energy barriers, as described in [270]. The calculated mechanisms also revealed the involvement of a C−N covalent bond prior to further reactions eventually leading to the formation of the N_2H^+, CH_3^+, $CH_3N_2^+$, and $CH_2N_2^+$ cations. When studying $[CH_4\cdots CH_4]^{2+}$ clusters, [271] found that the cluster would stabilize into a C−C bond and thence produce some of the first light hydrocarbon cationic precursors. The role divalent ionization chemistry may thus play in Titan and other planetary atmospheric chemistry is still largely unexplored but deserve further scrutiny, particularly since the double ionization thresholds of simple hydrocarbons, relevant to reduced atmospheres, are relatively small when placed in the context of upper atmospheres where higher-energy (>40 eV) electrons and photons (VUV–X-ray) precipitate. These processes underscore the need to experimentally and computationally explore ionized chemistry induced by electron and photon impact as divalent A^{++} ionization pathways are likely to be relevant the upper planetary atmospheres as an overlooked phenomenon participating in organic growth [269]. Finally, although at much higher electron impact energies

(300 eV), the $C_2H_6^{2+}$ dication was found to yield H_3^+ by vertical ionization [185]. Whether these processes would also occur on Uranus is at present a mystery, although the Earth, Mars, Venus, and Titan are all thought to harbor these dications [269]. Future constraints on these ionization processes are very relevant also in the context of data analysis, since mission mass spectrometry instruments (e.g., INMS and CAPS on Cassini) have not had a high enough mass resolution to distinguish between very close nuclear mass defects [269]. As a result, negative ion mass spectra analysis and interpretation have, for example, traditionally relied on assuming singly charged ions when conducting energy-to-mass data analyses [199]. Such an assumption may be acceptable for low-mass species but loses its validity for larger molecular species and photochemical aerosols.

4. Negative Ion Chemistry and Haze Growth

4.1. Anions on Titan

For many years, anion chemistry had remained constrained primarily to Earth's atmosphere where O (an electronegative species) atoms located in the ionosphere would undergo electron attachment reactions in the D-region, the lower part of the ionosphere <100 km [272]. Outside of Earth, negative ions have also been detected in comet Halley's inner coma (e.g., [273]), in the Enceladus polar plume [274], and finally on Titan [199,275–277]. Early photochemical models did not include anion chemistry (e.g., [95,135]) and it would not be until the 2007 when the discovery of very large negative ions, first up to *m/z* (mass/charge) of 10,000 [199] and then *m/z* 13,800 by [276], that our understanding of haze growth on Titan expanded and enabled photochemical models to incorporate the first steps of an unexplored chemistry [129,278]. Several anion-neutral mechanisms have been incorporated into photochemical models [70]. While photoionization processes mainly lead to the formation of primary ions such as N_2^+, CH_3^+, or H, anions can form through dissociative attachment of electrons with suprathermal electrons [278–280] including:

$$CH_4 + e^- \longrightarrow CH_2^- + H_2 \ (10.3\ \text{eV}) \quad (18)$$

$$C_2H_2 + e^- \longrightarrow C_2H^- + H \ (2.7\ \text{eV}) \quad (19)$$

Ion-pair formation,

$$H_2 + h\nu \longrightarrow H^- + H^+ \ (17.3\ \text{eV}) \quad (20)$$

$$CH_4 + h\nu \longrightarrow H^- + CH_3^+ \ (21.5\ \text{eV}) \quad (21)$$

Radiative electron attachment with thermal electrons,

$$H + e_{Th}^- \longrightarrow H^- + h\nu \quad (22)$$

And proton abstraction,

$$C_2H_2 + H^- \longrightarrow C_2H^- + H_2 \ (k = 4.4 \times 10^{-9}) \quad (23)$$

DEA reactions are strongly dependent on accurate reaction rate coefficients and photoabsorption and photoionization cross-sections ([70], *and references therein*). For most molecules considered in Titan photochemical schemes (e.g., HCN, HC_3N, and C_4H_2), DEA cross-sections reach maximum values at low energies (<7 eV) [127]. The DEA of methane is strongly cross-section-dependent, as seen in [127]. Depending on the DEA cross-sections used, even one or two orders of magnitude differences can induce large variations in

calculated mole fractions [127]. Thus, reducing uncertainties in these cross-sections is fundamental since anion products will directly participate in the organics and haze growth. The production of the simple hydride anion (Reactions (20) and (24)), of prime interstellar interest [281], is strongly model-dependent and an important precursor since it drives many of the proton abstraction reactions leading to the larger anionic C2, C3, and C4 species [10,127,278,282]. Thence, even with relatively low electron affinities, species such as H^- may present abundances higher than expected, considering the non-negligible CH_4 abundance in the atmosphere, generally slightly less abundant than the dominant CN^-. While direct abundance measurements by Cassini of H^- were not feasible [277], the degree of competition between DEA and proton abstraction of neutrals by H^- remains uncertain, resulting in model-observation discrepancies [126]. Experimental measurements of H^- desorption from *tholin* aerosol analogues from 3 to 15 eV electron irradiation could hint at the hydride anion being a key species incorporated into the photochemical haze [283]. Table 9 shows the dominant anion production and loss pathways near Titan's ionospheric peak at 1100 km.

$$CH_4 + e^- \longrightarrow H^- + CH_3 \quad (24)$$

Reaction pathways involving larger molecular compounds (>C3) become even more unresolved since these usually rely on slow and scant radiative attachment reactions (Reaction (25), see [284]). The study of these pathways has recently increased, benefiting from the detection of several anions in the ISM [281].

$$C_4H + e^- \longrightarrow C_4H^- + h\nu \quad (25)$$

Table 9. Dominant production (first row of each species) and loss (second row of each species) mechanisms for negative ions on Titan at 1100 km inside the ionosphere. Reaction rate coefficients are given in $cm^3\ s^{-1}$.

Species	Reaction	Rates ($cm^3\ s^{-1}$)	Ref.
H^-	$CH_4 + e^- \rightarrow H^- + CH_3$	(4.13×10^{-11})	[285]
	$H^- + h\nu \rightarrow H + e$	(1.81×10^{-2})	Miller-threshold Law
CN^-	$H^- + HCN \rightarrow CN^- + H_2$	1.50×10^{-8}	[286]
	$CN^- + H \rightarrow HCN + e$	6.30×10^{-10}	[286]
C_2H^-	$H^- + C_2H_2 \rightarrow C_2H^- + H_2$	3.10×10^{-9}	[282]
	$C_2H^- + H \rightarrow C_2H_2 + e$	1.60×10^{-9}	[287]
C_3N^-	$C_3N + e \rightarrow C_3N^- + h\nu$	2.63×10^{-10}	[288]
	$C_3N^- + H \rightarrow HC_3N$	5.4×10^{-10}	[289]
C_5N^-	$CN^- + HC_5N \rightarrow C_5N^- + HCN$	5.4×10^{-9}	Su-Chesnavich
	$C_5N^- + H \rightarrow HC_5N$	5.8×10^{-10}	[289]
C_4H^-	$C_4H + e \rightarrow C_4H^- + h\nu$	1.1×10^{-8}	[288]
	$C_4H^- + H \rightarrow C_2H_2 + e$	8.3×10^{-9}	[287]
C_6H^-	$H^- + C_6H_2 \rightarrow C_6H^- + H_2$	6.3×10^{-9}	Langevin
	$C_6H^- + H \rightarrow$ Products	5.0×10^{-10}	[287]
OH^-	$H^- + H_2O \rightarrow OH^- + H_2$	4.8×10^{-9}	[282]
	$OH^- + h\nu \rightarrow OH + e$	7.4×10^{-3}	Miller-threshold Law
O^-	$H_2O + e \rightarrow O^- + H_2$	(6.56×10^{-12})	[290]
	$O^- + h\nu \rightarrow O + e$	(1.04×10^{-2})	Miller-threshold Law

Other bimolecular negative ion reactions, such as associative detachment and cation+anion reactions also exist but the latter are generally less favorable than the afore-

mentioned pathways for the formation of anions on Titan [10]. For a complete reaction network review, the reader is referred to [70]. Associative electron detachment have been considered in all recent photochemical models, and rely mainly on the presence of the two most abundant radical species [278] in Titan's atmosphere: H and CH_3 [70,278], following Reaction (26). There exists an important knowledge gap pertaining to these reactions and in particular rate constants of associative detachment reactions, and ion-neutral reactions with H and CH_3 have been assumed to be the same [278]. A full bottom-up molecular growth promoted by anions is far from clear, especially given the difficulty in capturing exact ion densities with photochemical models [70]. To shed light on Titan's anion composition, few laboratory studies have investigated both low-mass and intermediate-mass species [291,292], but it appears that nitrogenated anions (N/C > 1) could play a role in the growth of *tholins* [292,293]. These studies have suggested that certain molecular candidates may even contain more than three nitrogen atoms, relatively stable in N- or H-rich environments [294].

$$A^- + B \rightarrow (AB^-)^* \rightarrow AB + e^- \quad (26)$$

4.2. Anions on Uranus

Negative ions in the atmosphere of Uranus have so far never been detected, let alone incorporated into photochemical models. In fact, their significance has been implicitly ruled out as early as 1977 [295], with the assumption of a very low abundance in the methyl radical CH_3 and atomic hydrogen H (and even an exclusion of CH_3 formation from the photochemical modeling of Neptune by [296]), thus possibly precluding efficient electron attachment reactions on Uranus. Radical chemistry is an important mechanism for the production of negative ions. The branching ratios and photoabsorption cross-sections of these radicals (and CH_4) are, however, either unknown or not fully characterized [144]. As seen on Titan previously, changes in these parameters may induce orders of magnitude variations in calculated ion densities. Furthermore, experimental work by [175] have underscored the photolytic efficiency of VUV and Ly-α radiation to generate CH_3 formation preferentially over the excited and ground-state of methylene $^1CH_2$ and $^3CH_2$, respectively. These branching ratios, if constrained accurately for the radiation conditions found at Uranus, may open a path for the formation of negative ions. Such pathways may further be possible depending on the variable solar input reaching Uranus. In addition, DEA mechanisms may also play a central role in Uranus's atmosphere, as was unexpectedly discovered on Titan, and ion-pair formation triggered by photon or electron impact are also a possibility [281]. In the latter case (Reactions (20) and (21)), the energy threshold is close to the parent neutral's ionization energy ($\sim$10 eV) which would make neutrals also exposed to ion-pair UV photo-destruction. Nevertheless, a strong lack in accurate absorption cross-sections, radical recombination rates (see [297]), and branching ratios renders any photochemical modeling task difficult to assess whether negative ions on Uranus play an important role in the photochemical haze growth, as is it expected on Titan. Future work in this field is much needed.

4.3. Summary: Dissociative Electron Attachment (<20 eV)

As an important source of negative ions production, DEA processes remain fundamental for photochemical models in order to calculate anion abundances [70]. However, these depend upon accurate cross-section measurements which can sometimes vary from one experimental technique to another [298]. In addition, these cross-sections are only available for a small number of hydrocarbons and N-bearing molecules relevant to planetary atmospheres, relying at times on estimates of other similar-sized hydrocarbons [298].

Table 10 lists a condensed and non-exhaustive summary of negative ion fragments produced through low-energy DEA processes.

Table 10. Low-energy dissociative electron attachment of 17 parent molecules relevant to the atmospheres of Titan and Uranus.

Parent	Fragment	Resonance Position (eV)	Cross-Section Peak (cm^2)	Refs.
CH_4	CH_2^-	10.4	1.4×10^{-19}	[127]
	H^-	9.8	1.6×10^{-18}	[127]
H_2	H^-	4.0	1.6×10^{-21}	[299]
		14	2.1×10^{-20}	[299]
D_2	D^-	14.0	5.5×10^{-21}	[299]
C_2H_2	C_2H^-	2.8	3.5×10^{-20}	[300]
	C_2^-	8.3	8.0×10^{-21}	[300]
	H^-	7.9	3.9×10^{-20}	[300]
C_2H_4	H^-	10.5	1.9×10^{-24}	[301,302]
	CH^-	9.8	*ion yield*	[302]
	C_2H^-	9.8	*ion yield*	[302]
	$C_2H_2^-$	1.6	*ion yield*	[302]
	$C_2H_3^-$	7.0	*ion yield*	[302]
C_2H_6	H^-	9.2	*ion yield*	[301]
C_3H_4	$C_3H_3^-$	3.4	1.9×10^{-24}	[303]
C_3H_8	H^-	8.6	*ion yield*	[301]
C_4H_2	C_4H^-	2.5	3.0×10^{-24}	[304]
		5.3	7.3×10^{-23}	[304]
C_4H_6	H^-	4.0	1.4×10^{-24}	[303]
C_6H_2	C_6H^-	2.8	3.5×10^{-20}, *est.*	[278,298,304]
HCN	CN^-	1.9	9.4×10^{-22}	[305]
DCN	CN^-	1.9	3.4×10^{-22}	[305]
NH_3	H^-	5.7	2.3×10^{-18}	[285]
	NH_2^-	5.9	1.6×10^{-18}	[285]
CH_2N_2	CN^-	6.4	3.9×10^{-20}	[306]
$C_2H_4N_2$	CN^-	1.9	3.9×10^{-20}	[307]
H_2S	HS^-	1.6	1.8×10^{-18}	[308,309]
	S^-	9.7	4.4×10^{-19}	[308,309]

Note: Certain experiments have provided the ion yields of fragments and these are annotated here. More DEA cross-section data can be found at the Innsbruck Dissociative Electron Attachment DataBase (IDEADB) node: https://ideadb.uibk.ac.at/, accessed on 9 June 2025.

5. Summary: Opportunities for Future Studies

The planetary atmospheres of the cold regions of the outer solar system provide a unique natural laboratory presenting a wide array of chemical compositions and atmosphere-magnetosphere interactions. The composition of these atmospheres is also prone to the variables of seasonal changes and exogenic material precipitation, both affecting their thermal, chemical, and physical characteristics. The succession of the Pioneer, Voyager, and Cassini-Huygens missions opened new pathways towards the characterization of the gas giants while simultaneously spawning even more questions on their origins and evolution. Uranus and Neptune, the two least explored planets in the solar system, likely portray features that will ultimately improve our understanding of the formation of our solar system and that of exoplanets, too. The Cassini mission in particular has unearthed an invaluable amount of discovery at Titan and will continue to provide the community with an ameliorated description of the global atmosphere, given of wealth of non-analyzed data. With Uranus being placed at a top priority for a future flagship mission [1], the available breadth of observational, theoretical, and experimental techniques

will help support the future investigation of the Uranian environment. As detailed in a recent community input poll, the interest in future Uranian studies encompasses a large scope of domains, from the study of the atmosphere, rings and satellites, the interior, and the magnetosphere [310]. This review attempts to describe the broad effects of photochemical processes induced by low-energy (<50 eV) photons and electrons on the growth of organic molecules in the gas and solid phases. Future synergistic work can help address many of the scientific questions and uncertainties laid out here, in order to better understand the formation mechanisms of organic molecules and chemically complex haze particles.

Funding: NASA SMD support for this work is acknowledged.

Acknowledgments: The author expresses gratitude to two anonymous reviewers who contributed to the improvement of this review through constructive remarks, and to the Guest Editor of this Special Issue, Hassan Abdoul-Carime. The author gratefully acknowledges insightful discussions with Lora Jovanovic and her assistance with figure improvements. Sincere appreciation is also extended to Benoît Seignovert, Nathalie Carrasco, Olivier Mousis, Mark Hofstadter, Michel Nuevo, Jean-Pierre Lebreton, Toshiaki Matsubara, Salma Bejaoui, Ella Sciamma-O'Brien, and Farid Salama for valuable scientific exchanges. The author is particularly thankful to Chris Arumainayagam for helpful guidance regarding low-energy electron interactions, and to Partha Bera for guidance in understanding vertical ionization processes. Special thanks are due to Christiaan Boersma for his consistent encouragement. The author also wishes to thank Mustapha Meftah for generously providing the high-resolution SOLAR-HRS SSI raw data. Deep gratitude is expressed to Hadir Marei for her foundational and ongoing motivation throughout the preparation of this work. Any oversights or errors remain the sole responsibility of the author. This work has made use of NASA's Astrophysics Data System. S.D.G.

Conflicts of Interest: The author declares no conflicts of interest.

Abbreviations

UOP	Uranus Orbiter Probe
GCR	Galactic Cosmic Rays
UVS	Ultraviolet Spectrometer
NUV	Near Ultraviolet
FUV	Far Ultraviolet
VUV	Vacuum Ultraviolet
EUV	Extreme Ultraviolet
LIPM	Local Interplanetary Medium
ISRF	Interstellar Radiation Field
ISM	Interstellar Medium
JWST	James Webb Space Telescope
CRIR	Cosmic Ray Ionization Rate
INMS	Ion and Neutral Mass Spectrometer
CAPS	Cassini Plasma Spectrometer
SSI	Solar Spectrum Irradiance
CCN	Cloud Condensation Nuclei
DEA	Dissociative Electron Attachment
TNI	Temporary Negative Ions

References

1. National Academies of Sciences, Engineering, and Medicine. *Origins, Worlds, and Life: A Decadal Strategy for Planetary Science and Astrobiology 2023–2032*; National Academies Press: Washington, DC, USA, 2023. [CrossRef]
2. Lebreton, J.P.; Matson, D.L. An overview of the Cassini mission. *Il Nuovo Cimento C* **1992**, *15*, 1137–1147. [CrossRef]
3. Lebreton, J.P.; Matson, D.L. The Huygens probe: Science, payload and mission overview. *Space Sci. Rev.* **2002**, *104*, 59–100. [CrossRef]

4. Lebreton, J.P.; Witasse, O.; Sollazzo, C.; Blancquaert, T.; Couzin, P.; Schipper, A.M.; Jones, J.B.; Matson, D.L.; Gurvits, L.I.; Atkinson, D.H.; et al. An overview of the descent and landing of the Huygens probe on Titan. *Nature* **2005**. *438*, 758–764. [CrossRef] [PubMed]
5. Brown, R.H.; Lebreton, J.P.; Waite, J. *Titan from Cassini-Huygens*; Springer: Berlin/Heidelberg, Germany, 2009.
6. Lopes, R.M.C.; Elachi, C.; Müller-Wodarg, I.C.F.; Solomonidou, A. *Titan After Cassini-Huygens*; Springer: Berlin/Heidelberg, Germany, 2025.
7. Cable, M.L.; Hörst, S.M.; Hodyss, R.; Beauchamp, P.M.; Smith, M.A.; Willis, P.A. Titan tholins: Simulating Titan organic chemistry in the Cassini-Huygens era. *Chem. Rev.* **2012**, *112*, 1882–1909. [CrossRef] [PubMed]
8. Hörst, S.M. Titan's Atmosphere and Climate. *J. Geophys. Res. Planets* **2017**, *122*, 432–482. [CrossRef]
9. Nixon, C.A.; Lorenz, R.D.; Achterberg, R.K.; Buch, A.; Coll, P.; Clark, R.N.; Courtin, R.; Hayes, A.; Iess, L.; Johnson, R.E.; et al. Titan's cold case files-Outstanding questions after Cassini-Huygens. *Planet. Space Sci.* **2018**, *155*, 50–72. [CrossRef]
10. Nixon, C.A. The Composition and Chemistry of Titan's Atmosphere. *ACS Earth Space Chem.* **2024**, *8*, 406–456 . [CrossRef]
11. Nixon, C.A.; Achterberg, R.K.; Ádámkovics, M.; Bézard, B.; Bjoraker, G.L.; Cornet, T.; Hayes, A.G.; Lellouch, E.; Lemmon, M.T.; López-Puertas, M.; et al. Titan Science with the James Webb Space Telescope. *Astron. Soc. Pac.* **2016**, *128*, 018009. [CrossRef]
12. Coy, B.P.; Nixon, C.A.; Rowe-Gurney, N.; Achterberg, R.; Lombardo, N.A.; Fletcher, L.N.; Irwin, P. Spitzer IRS Observations of Titan as a Precursor to JWST MIRI Observations. *Planet. Sci. J.* **2023**, *4*, 114. [CrossRef]
13. Goldreich, P.; Lithwick, Y.; Sari, R. Planet Formation by Coagulation: A Focus on Uranus and Neptune. *Annu. Rev. Astron. Astrophys.* **2004**, *42*, 549–601. [CrossRef]
14. Helled, R.; Bodenheimer, P. The Formation of Uranus and Neptune: Challenges and Implications for Intermediate-mass Exoplanets. *Astrophys. J.* **2014**, *789*, 69. [CrossRef]
15. Guillot, T. Uranus and Neptune are key to understand planets with hydrogen atmospheres. *Exp. Astron.* **2019**, *54*, 1027–1049. [CrossRef]
16. Moses, I.; Allen, M. Nucleation and Aerosol Formation Neptune's Atmosphere . *Icarus* **1992**, *346*, 318–346. [CrossRef]
17. Orton, G.S.; Fletcher, L.N.; Moses, J.I.; Mainzer, A.K.; Hines, D.; Hammel, H.B.; Martin-Torres, F.J.; Burgdorf, M.; Merlet, C.; Line, M.R. Mid-Infrared Spectroscopy of Uranus from the Spitzer Infrared Spectrometer: 1. Determination of the Mean Temperature Structure of the Upper Troposphere and Stratosphere. *Icarus* **2014**, *243*, 494–513. [CrossRef]
18. Moses, J.I. ; Fletcher, L.N.; Greathouse, T.K.; Orton, G.S.; Hue, V. Seasonal stratospheric photochemistry on Uranus and Neptune. *Icarus* **2018**, *307*, 124–145. [CrossRef]
19. Hueso, R.; Sánchez-Lavega, A. Atmospheric Dynamics and Vertical Structure of Uranus and Neptune's Weather Layers. *Space Sci. Rev.* **2019**, *215*, 52. [CrossRef]
20. Moses, J.I.; Cavalié, T.; Fletcher, L.N.; Roman, M.T. Atmospheric chemistry on Uranus and Neptune. *Philos. Trans. R. Soc. A Math. Phys. Eng. Sci.* **2020**, *378*, 20190477. [CrossRef]
21. Fletcher, L.N. The Atmosphere of Uranus. In *Oxford Research Encyclopedia of Planetary Science*; Oxford University Press: Oxford, UK, 2021.
22. Lamy, L.; Prangé, R.; Hansen, K.C.; Clarke, J.T.; Zarka, P.; Cecconi, B.; Aboudarham, J.; André, N.; Branduardi-Raymont, G.; Gladstone, R.; et al. Earth-based detection of Uranus' aurorae. *Geophys. Res. Lett.* **2012**, *39, L07105*. [CrossRef]
23. Melin, H. The upper atmospheres of Uranus and Neptune. *Philos. Trans. R. Soc. A* **2020**, *378*, 20190478. [CrossRef]
24. Broadfoot, A.L.; Atreya, S.K.; Bertaux, J.L.; Blamont, J.E.; Dessler, A.J.; Donahue, T.M.; Forrester, W.T.; Hall, D.T.; Herbert, F.; Holberg, J.B.; et al. Ultraviolet Spectrometer Observations of Neptune and Triton. *Science* **1989**, *246*, 1459–1466. [CrossRef]
25. Moore, L.; Moses, J.I.; Melin, H.; Stallard, T.S.; O'Donoghue, J. Atmospheric implications of the lack of H_3^+ detection at Neptune. *Philos. Trans. R. Soc. A Math. Phys. Eng. Sci.* **2020**, *378*, 20200100. [CrossRef]
26. Strobel, D.F.; Yelle, R.V.; Shemansky, D.E.; Atreya, S.K. The Upper Atmosphere of Uranus. In *Uranus*; The University of Arizona Press: Tucson, AZ, USA, 1991.
27. Atreya, S.K.; Sandel, B.R.; Romani, P.N. Photochemistry and Vertical Mixing. In *Uranus*; The University of Arizona Press: Tucson, AZ, USA, 1991.
28. Orton, G.S.; Baines, K.H.; Caldwell, J.; Romani, P.; Tokunaga, A.T.; West, R.A. Calibration of the 7- to 14-μm brightness spectra of Uranus and Neptune. *Icarus* **1990**, *85*, 257–265. [CrossRef]
29. Encrenaz, T.; Feuchtgruber, H.; Atreya, S.K.; Bézard, B.; Lellouch, E.; Bishop, J.; Edgington, S.; De Graauw, T.; Griffin, M.; Kessler, M.F. ISO observations of Uranus: The stratospheric distribution of C_2H_2 and the eddy diffusion coefficient. *Astron. Astrophys.* **1998**, *333*, L43–L46.
30. Pearl, J.; Conrath, B.; Hanel, R.; Pirraglia, J.; Coustenis, A. The albedo, effective temperature, and energy balance of Uranus, as determined from Voyager IRIS data. *Icarus* **1990**, *84*, 12–28. [CrossRef]
31. Wang, X.; Li, L.; Roman, M.; Zhang, X.; Jiang, X.; Fry, P.M.; Li, C.; Milcareck, G.; Sanchez-Lavega, A.; Perez-Hoyos, S.; et al. Internal Heat and Energy Imbalance of Uranus. *arXiv* **2025**, arXiv:2502.20722. [CrossRef]

32. Sromovsky, L.; Karkoschka, E.; Fry, P.; de Pater, I.; Hammel, H. The methane distribution and polar brightening on Uranus based on HST/STIS, Keck/NIRC2, and IRTF/SpeX observations through 2015. *Icarus* **2019**, *317*, 266–306. [CrossRef]
33. Yelle, R.V.; Doose, L.R.; Tomasko, M.G.; Strobel, D.F. Analysis of Raman scattered LY-α emissions from the atmosphere of Uranus. *Geophys. Res. Lett.* **1987**, *14*, 483–486. [CrossRef]
34. Herbert, F.; Sandel, B.R.; Yelle, R.V.; Holberg, J.B.; Broadfoot, A.L.; Shemansky, D.E.; Atreya, S.K.; Romani, P.N. The upper atmosphere of Uranus: EUV occultations observed by Voyager 2. *J. Geophys. Res. Space Phys.* **1987**, *92*, 15093–15109. [CrossRef]
35. Yelle, R.V.; McConnell, J.C.; Strobel, D.F.; Doose, L.R. The far ultraviolet reflection spectrum of Uranus: Results from the Voyager encounter. *Icarus* **1989**, *77*, 439–456. [CrossRef]
36. Barthélemy, M.; Lamy, L.; Menager, H.; Schulik, M.; Bernard, D.; Abgrall, H.; Roueff, E.; Cessateur, G.; Prange, R.; Lilensten, J. Dayglow and auroral emissions of Uranus in H2 FUV bands. *Icarus* **2014**, *239*, 160–167. [CrossRef]
37. Waite, J.H.; Chandler, M.O.; Yelle, R.V.; Sandel, B.R.; Cravens, T.E. Superthermal electron processes in the upper atmosphere of Uranus: Aurora and electroglow. *J. Geophys. Res. Space Phys.* **1988**, *93*, 14295–14308. [CrossRef]
38. Barthélemy, M.; Cessateur, G. Sensitivity of upper atmospheric emissions calculations to solar/stellar UV flux. *J. Space Weather Space Clim.* **2014**, *4*, A35. [CrossRef]
39. France, K.; Froning, C.S.; Linsky, J.L.; Roberge, A.; Stocke, J.T.; Tian, F.; Bushinsky, R.; Désert, J.M.; Mauas, P.; Vieytes, M.; et al. The Ultraviolet Radiation Environment Around M Dwarf Exoplanet Host Stars. *Astrophys. J.* **2013**, *763*, 149. [CrossRef]
40. Linsky, J.L.; France, K.; Ayres, T. Computing Intrinsic LYα Fluxes of F5 V to M5 V Stars. *Astrophys. J.* **2013**, *766*, 69. [CrossRef]
41. Linsky, J.L.; Redfield, S. Inferring Intrinsic Stellar EUV and Lyman-Alpha Fluxes and Their Effects on Exoplanet Atmospheres. *Space Sci. Rev.* **2024**, *220*, 32. [CrossRef]
42. Meftah, M.; Sarkissian, A.; Keckhut, P.; Hauchecorne, A. The SOLAR-HRS New High-Resolution Solar Spectra for Disk-Integrated, Disk-Center, and Intermediate Cases. *Remote Sens.* **2023**, *15*, 3560. [CrossRef]
43. Secchi, A. Resultats fournis par l'analyse spectrale de la lumiere d'Uranus, de l'étoile R des Gémeaus, et des taches solaires. *Comptes Rendus* **1869**, *68*, 761–765.
44. Huggins, W. IV. Note on the spectrum of Uranus and the spectrum of comet I., 1871. *Proc. R. Soc. Lond.* **1871**, *19*, 488–491. [CrossRef]
45. Chinnici, I. Contributions to Astrophysics and other Sciences. In *Decoding the Stars: A Biography of Angelo Secchi, Jesuit and Scientist*; BRILL: Leiden, The Netherlands, 2019; pp. 160–207. [CrossRef]
46. Adel, A.; Slipher, V.M. The Constitution of the Atmospheres of the Giant Planets. *Phys. Rev.* **1934**, *46*, 902–906. [CrossRef]
47. Herzberg, G.; Welsh, H.L.; Crawford, M.F.; F MacDonald, J.C.; Chisholm, D.A. Spectroscopic Evidence of Molecular Hydrogen in the Atmospheres of Uranus and Neptune. *Astrophys. J.* **1952** , *115*, 337–340. [CrossRef]
48. Encrenaz, T.; Combes, M.; Atreya, S.K.; Romani, P.N.; Fricke, K.; Moore, V.; Hunt, G.; Wagener, R.; Caldwell, J.; Owen, T.; et al. A study of the upper atmosphere of Uranus using the IUE. *Astron. Astrophys.* **1986**, *162*, 317–322.
49. Tyler, G.L. ; Sweetnam, D.N.; Anderson, J.D.; Campbell, J.K.; Eshleman, V.R.; Hinson, D.P.; Levy, G.S.; Lindal, G.F.; Marouf, E.A.; Simpson, R.A. Voyager 2 Radio Science Observations of the Uranian System: Atmosphere, Rings, and Satellites. *Science* **1986**, *233*, 79–84. [CrossRef]
50. Conrath, B.; Gautier, D.; Hanel, R.; Lindal, G.; Marten, A. The helium abundance of Uranus from Voyager measurements. *J. Geophys. Res. Space Phys.* **1987**, *92*, 15003–15010. [CrossRef]
51. Encrenaz, T.; Lellouch, E.; Drossart, P.; Feuchtgruber, H.; Orton, G.S.; Atreya, S.K. First detection of CO in Uranus. *Astron. Astrophys.* **2004**, *413*, L5–L9. [CrossRef]
52. Burgdorf, M.; Orton, G.; van Cleve, J.; Meadows, V.; Houck, J. Detection of new hydrocarbons in Uranus' atmosphere by infrared spectroscopy. *Icarus* **2006**, *184*, 634–637. [CrossRef]
53. Moreno, R.; Lellouch, E.; Cavalié, T.; Moullet, A. Detection of CS in Neptune's atmosphere from ALMA observations. *Astron. Astrophys.* **2017**, *608*, L5. [CrossRef]
54. Irwin, P.G.J.; Toledo, D.; Garland, R.; Teanby, N.A.; Fletcher, L.N.; Orton, G.A.; Bézard, B. Detection of hydrogen sulphide above the clouds in Uranus' atmosphere. *Nat. Astron.* **2018**, *2*, 420–427. [CrossRef]
55. Karkoschka, E.; Tomasko, M. The haze and methane distributions on Uranus from HST-STIS spectroscopy. *Icarus* **2009**, *202*, 287–309. [CrossRef]
56. Lunine, J.I. The Atmospheres of Uranus and Neptune. *Annu. Rev. Astron. Astrophys.* **1993**, *31*, 217–263. [CrossRef]
57. Irwin, P.G.J.; Teanby, N.A.; Fletcher, L.N.; Toledo, D.; Orton, G.S.; Wong, M.H.; Roman, M.T.; Pérez-Hoyos, S.; James, A.; Dobinson, J. Hazy Blue Worlds A Holistic Aerosol Model for Uranus and Neptune Including Dark Spots. *JGR Planets* **2022**, *127*, e2022JE007189. [CrossRef]
58. Sánchez-Lavega, A.; Irwin, P.; García Muñoz, A. Dynamics and clouds in planetary atmospheres from telescopic observations. *Astron. Astrophys. Rev.* **2023**, *31*, 5. [CrossRef]

59. Irwin, P.G.; Dobinson, J.; James, A.; Teanby, N.A.; Simon, A.A.; Fletcher, L.N.; Roman, M.T.; Orton, G.S.; Wong, M.H.; Toledo, D.; et al. Modelling the seasonal cycle of Uranus's colourānd magnitude,ānd comparison with Neptune. *Mon. Not. R. Astron. Soc.* **2024**, *527*, 11521–11538. [CrossRef]
60. Fegley, B.J.; Gautier, D.; Owen, T.; Prinn, R.G. Spectroscopy and Chemistry of the Atmosphere of Uranus. In *Uranus*; Bergstralh, J.T., Miner, E.D., Matthews, M.S., Eds.; The University of Arizona Press: Tucson, AZ, USA, 1991.
61. Vorburger, A.; Wurz, P.; Helled, R.; Mousis, O. Mass Spectrometer Experiment for a Uranus Probe. *Space Sci. Rev.* **2024**, *220*, 64. [CrossRef]
62. Molina-Cuberos, G.J.; Witasse, O.; Toledo, D.; Tripathi, S.N. The Low-Altitude Ionosphere of the Ice Giant Planets. *J. Geophys. Res. Planets* **2023**, *128*, e2022JE007568. [CrossRef]
63. Mousis, O.; Atkinson, D.H.; Cavalié, T.; Fletcher, L.N.; Amato, M.J.; Aslam, S.; Ferri, F.; Renard, J.B.; Spilker, T.; Venkatapathy, E.; et al. Scientific rationale for Uranus and Neptune in situ explorations.*Planet. Space Sci.* **2018**, *155*, 12–40. [CrossRef]
64. Apéstigue, V.; Toledo, D.; Irwin, P.G.; Rannou, P.; Gonzalo, A.; Martínez-Oter, J.; Ceballos-Cáceres, J.; Azcue, J.; Jiménez, J.J.; Sebastian, E.; et al. The Uranus Multi-Experiment Radiometer for Haze and Clouds Characterization. *Space Sci. Rev.* **2024**, *220*, 6. [CrossRef]
65. Niemann, H.B.; Atreya, S.K.; Bauer, S.J.; Carignan, G.R.; Demick, J.E.; Frost, R.L.; Gautier, D.; Haberman, J.A.; Harpold, D.N.; Hunten, D.M.; et al. The abundances of constituents of Titan's atmosphere from the GCMS instrument on the Huygens probe. *Nature* **2005**, *438*, 779–784. [CrossRef]
66. Fletcher, L.; Orton, G.; Teanby, N.; Irwin, P.; Bjoraker, G. Methane and its isotopologues on Saturn from Cassini/CIRS observations. *Icarus* **2009**, *199*, 351–367. [CrossRef]
67. Howett, C.; Irwin, P.; Teanby, N.; Simon-Miller, A.; Calcutt, S.; Fletcher, L.; De Kok, R. Meridional variations in stratospheric acetylene and ethane in the southern hemisphere of the saturnian atmosphere as determined from Cassini/CIRS measurements. *Icarus* **2007**, *190*, 556–572. [CrossRef]
68. Guerlet, S.; Fouchet, T.; Bézard, B. Ethane, Acetylene and Propane distribution in Saturn's Stratosphere from Cassini/CIRS Limb Observations. In Proceedings of the SF2A-2008: Proceedings of the Annual Meeting of the French Society of Astronomy and Astrophysics, Paris, France, 30 June–4 July 2008.
69. Sylvestre, M.; Guerlet, S.; Fouchet, T.; Spiga, A.; Flasar, F.; Hesman, B.; Bjoraker, G. Seasonal changes in Saturn's stratosphere inferred from Cassini/CIRS limb observations. *Icarus* **2015**, *258*, 224–238. [CrossRef]
70. Vuitton, V.; Yelle, R.V.; Klippenstein, S.J.; Hörst, S.M.; Lavvas, P. Simulating the density of organic species in the atmosphere of Titan with a coupled ion-neutral photochemical model. *Icarus* **2019**, *324*, 120–197. [CrossRef]
71. Hesman, B.E.; Bjoraker, G.L.; Sada, P.V.; Achterberg, R.K.; Jennings, D.E.; Romani, P.N.; Lunsford, A.W.; Fletcher, L.N.; Boyle, R.J.; Simon-Miller, A.A.; et al. Elusive Ethylene Detected in Saturn's Northern Storm Region. *Astrophys. J.* **2012**, *760*, 24. [CrossRef]
72. Guerlet, S.; Fouchet, T.; Bézard, B.; Moses, J.I.; Fletcher, L.N.; Simon-miller, A.A.; Flasar, F.M. Meridional distribution of CH3C2H and C4H2 in Saturn's stratosphere from CIRS/Cassini limb and nadir observations. *Icarus* **2010**, *209*, 682–695. [CrossRef]
73. Abbas, M.M.; LeClair, A.; Woodard, E.; Young, M.; Stanbro, M.; Flasar, M. Measurements of CO2 Distribution in Saturn's Atmosphere by Cassini-Infrared Observations. In Proceedings of the 44th Lunar and Planetary Science Conference (LPSC), The Woodlands, TX, USA, 18–22 March 2013.
74. Cavalié, T.; Billebaud, F.; Dobrijevic, M.; Fouchet, T.; Lellouch, E.; Encrenaz, T.; Brillet, J.; Moriarty-Schieven, G.; Wouterloot, J.; Hartogh, P. First observation of CO at 345GHz in the atmosphere of Saturn with the JCMT: New constraints on its origin. *Icarus* **2009**, *203*, 531–540. [CrossRef]
75. Cavalié, T.; Hue, V.; Hartogh, P.; Moreno, R.; Lellouch, E.; Feuchtgruber, H.; Jarchow, C.; Cassidy, T.; Fletcher, L.N.; Billebaud, F.; et al. Herschel map of Saturn's stratospheric water, delivered by the plumes of Enceladus. *Astron. Astrophys.* **2019**, *630*, A87. [CrossRef]
76. Coustenis, A.; Jennings, D.E.; Jolly, A.; Bénilan, Y.; Nixon, C.A.; Vinatier, S.; Gautier, D.; Bjoraker, G.L.; Romani, P.N.; Carlson, R.C.; et al. Detection of C2HD and the D/H ratio on Titan. *Icarus* **2008**, *197*, 539–548. [CrossRef]
77. Pierel, J.D.R.; Nixon, C.A.; Lellouch, E.; Fletcher, L.N.; Bjoraker, G.L.; Achterberg, R.K.; Bézard, B.; Hesman, B.E.; Irwin, P.G.J.; Flasar, F.M. D/H Ratios on Saturn and Jupiter from Cassini CIRS. *Astron. J.* **2017**, *154*, 178. [CrossRef]
78. Atreya, S.K.; Ponthieu, J.J. Photolysis of Methane and the Ionosphere of Uranus. *Planet. Space Sci.* **1983**, *31*, 939. [CrossRef]
79. Summers, M.E.; Strobel, D.F. Photochemistry of the Atmosphere of Uranus. *Astrophys. J.* **1989**, *346*, 495–508. [CrossRef]
80. Romani, P.N.; Bishop, J.; Bézard, B.; Atreya, S. Methane Photochemistry on Neptune: Ethane and Acetylene Mixing Ratios and Haze Production. *Icarus* **1993**, *106*, 442–463. [CrossRef]
81. Lellouch, E.; Romani, P.N.; Rosenqvist, J. The vertical Distribution and Origin of HCN in Neptune's Atmosphere. *Icarus* **1994**, *108*, 112–136. [CrossRef]
82. Dobrijevic, M.; Cavali, T.; Hbrard, E.; Billebaud, F.; Hersant, F.; Selsis, F. Key reactions in the photochemistry of hydrocarbons in Neptune's stratosphere. *Planet. Space Sci.* **2010**, *58*, 1555–1566. [CrossRef]

83. Cavalié, T.; Moreno, R.; Lellouch, E.; Hartogh, P.; Venot, O.; Orton, G.S.; Jarchow, C.; Encrenaz, T.; Selsis, F.; Hersant, F.; et al. The first submillimeter observation of CO in the stratosphere of Uranus. *Astron. Astrophys.* **2014**, *562*, A33. [CrossRef]
84. Moses, J.I.; Poppe, A.R. Dust ablation on the giant planets: Consequences for stratospheric photochemistry. *Icarus* **2017**, *297*, 33–58. [CrossRef]
85. Milcareck, G.; Guerlet, S.; Montmessin, F.; Spiga, A.; Leconte, J.; Millour, E.; Clément, N.; Fletcher, L.N.; Roman, M.T.; Lellouch, E.; et al. Radiative-convective models of the atmospheres of Uranus and Neptune: Heating sources and seasonal effects. *Astron. Astrophys.* **2024**, *686*, A303. [CrossRef]
86. Waite, J.H.; Young, D.; Cravens, T.E.; Coates, A.J.; Crary, F.J.; Magee, B.; Westlake, J. The Process of Tholin Formation in Titan's Upper Atmosphere. *Science* **2007**, *316*, 870–875. [CrossRef] [PubMed]
87. Krasnopolsky, V.A. Chemical composition of Titan's atmosphere and ionosphere: Observations and the photochemical model. *Icarus* **2014**, *236*, 83–91. [CrossRef]
88. Plainaki, C.; Lilensten, J.; Radioti, A.; Andriopoulou, M.; Milillo, A.; Nordheim, T.A.; Dandouras, I.; Coustenis, A.; Grassi, D.; Mangano, V.; et al. Planetary space weather: Scientific aspects and future perspectives. *J. Space Weather Space Clim.* **2016**, *6*, A31. [CrossRef]
89. Crary, F.J.; Magee, B.A.; Mandt, K.; Waite, J.H.; Westlake, J.; Young, D.T. Heavy ions, temperatures and winds in Titan's ionosphere: Combined Cassini CAPS and INMS observations. *Planet. Space Sci.* **2009**, *57*, 1847–1856. [CrossRef]
90. Cui, J.; Galand, M.; Yelle, R.V.; Vuitton, V.; Wahlund, J.; Lavvas, P.P. Diurnal variations of Titan's ionosphere. *J. Geophys. Res.* **2009**, *114*, 1–20. [CrossRef]
91. Cui, J.; Yelle, R.V.; Vuitton, V.; Waite, J.H.; Kasprzak, W.T.; Gell, D.A.; Niemann, H.B.; Müller-Wodarg, I.C.F.; Borggren, N.; Fletcher, G.G.; et al. Analysis of Titan's neutral upper atmosphere from Cassini Ion Neutral Mass Spectrometer measurements. *Icarus* **2009**, *200*, 581–615. [CrossRef]
92. Dubois, D. Study of Titan's Upper and Lower Atmosphere: An Experimental Approach. Ph.D. Thesis, Université Paris Saclay, Orsay, France, 2018.
93. Broadfoot, A.L.; Sandel, B.R.; Shemansky, D.; Holberg, J.B.; Smith, G.R. Extreme Ultraviolet Observations from Voyager 1 Encounter with Saturn. *Science* **1981**, *212*, 206–211. [CrossRef] [PubMed]
94. Keller, C.N.; Cravens, T.E.; Gan, L. A model of the ionosphere of Titan. *J. Geophys. Res. Space Phys.* **1992**, *97*, 12117–12135. [CrossRef]
95. Yung, Y.L.; Allen, M.; Pinto, J. Photochemistry of the atmosphere of Titan: Comparison between model and observations. *Astrophys. J.* **1984**, *212*, 465–506. [CrossRef]
96. Singhal, R.P.; Haider, S.A. Some Molecular Nitrogen Emissions from Titan-Solar EUV and Magnetospheric Interaction. *Indian J. Radio Space Phys.* **1986**, *15*, 46–52 .
97. Yung, Y.L. An update of nitrile photochemistry on Titan. *Icarus* **1987**, *72*, 468–472. [CrossRef]
98. Ip, W.H. Titan's upper ionosphere. *Astrophys. J.* **1990**, *362* , 354–363. [CrossRef]
99. Gan, L.; Keller, C.N.; Cravens, T.E. Electrons in the Ionosphere of Titan. *J. Geophys. Res.* **1992**, *97*, 12137–12151 . [CrossRef]
100. Keller, C.N.; Anicich, V.G.; Cravens, T.E. Model of Titan's ionosphere with detailed hydrocarbon ion chemistry. *Planet. Space Sci.* **1998**, *46*, 1157–1174. [CrossRef]
101. Lavvas, P.P.; Coustenis, A.; Vardavas, I.M. Coupling photochemistry with haze formation in Titan's atmosphere, Part I: Model description. *Planet. Space Sci.* **2008**, *56*, 67–99. [CrossRef]
102. Thuillier, G.; Floyd, L.; Woods, T.; Cebula, R.; Hilsenrath, E.; Hersé, M.; Labs, D. Solar irradiance reference spectra for two solar active levels. *Adv. Space Res.* **2004**, *34*, 256–261. [CrossRef]
103. Lavvas, P.; Galand, M.; Yelle, R.V.; Heays, A.N.; Lewis, B.R.; Lewis, G.R.; Coates, A.J. Energy deposition and primary chemical products in Titan's upper atmosphere. *Icarus* **2011**, *213*, 233–251. [CrossRef]
104. Couturier-Tamburelli, I.; Gudipati, M.S.; Lignell, A.; Jacovi, R.; Piétri, N. Spectroscopic studies of non-volatile residue formed by photochemistry of solid C4N2: A model of condensed aerosol formation on Titan. *Icarus* **2014**, *234*, 81–90. [CrossRef]
105. Hébrard, E. Incertitudes Photochimiques Dans les Modèles de L'atmosphère de Titan : Revue et Conséquences. Ph.D. Thesis, Université Paris-Diderot-Paris, Paris, France, 2006.
106. Anderson, C.M.; Samuelson, R.E.; Nna-Mvondo, D. Organic Ices in Titan's Stratosphere. *Space Sci. Rev.* **2018**, *214*, 125. [CrossRef]
107. Barth, E.L. Modeling survey of ices in Titan's stratosphere. *Planet. Space Sci.* **2017**, *137*, 20–31. [CrossRef]
108. Anderson, C.M.; Samuelson, R.E.; Yung, Y.L.; McLain, J.L. Solid-state chemistry as a formation mechanism for Titan's stratospheric C4N2 ice clouds. *Geophys. Res. Lett.* **2016**, *43*, 3088–3094. [CrossRef]
109. Nna-Mvondo, D.; Anderson, C.; Samuelson, R.E. *CIRS-Observed Titan's Stratospheric Ice Clouds Studied in the Laboratory*; American Astronomical Society: Washington, DC, USA, 2018.
110. De Kok, R.J.; Teanby, N.A.; Maltagliati, L.; Irwin, P.G.J.; Vinatier, S. HCN ice in Titan's high-altitude southern polar cloud. *Nature* **2014**, *514*, 65–67. [CrossRef] [PubMed]

111. Vinatier, S.; Schmitt, B.; Bézard, B.; Rannou, P.; Dauphin, C.; de Kok, R.; Jennings, D.E.; Flasar, F.M. Study of Titan's fall southern stratospheric polar cloud composition with Cassini/CIRS: Detection of benzene ice. *Icarus* **2018**, *310* , 89–104. [CrossRef]
112. Rodriguez, S.; Le Mouélic, S.; Rannou, P.; Tobie, G.; Baines, K.H.; Barnes, J.W.; Griffith, C.A.; Hirtzig, M.; Pitman, K.M.; Sotin, C.; et al. Global circulation as the main source of cloud activity on Titan. *Nature* **2009**, *459*, 678–682. [CrossRef]
113. Lora, J.M.; Lunine, J.I.; Russell, J.L. GCM simulations of Titan's middle and lower atmosphere and comparison to observations. *Icarus* **2015**, *250*, 516–528. [CrossRef]
114. Barth, E. Planetcarma: A new framework for studying the microphysics of planetary atmospheres. *Atmosphere* **2020**, *11*, 1064 . [CrossRef]
115. Dubois, D.; Iraci, L.T.; Barth, E.L.; Salama, F.; Vinatier, S.; Sciamma-O'Brien, E. Investigating the condensation of benzene (C6H6) in Titan's South polar cloud system with a combination of laboratory, observational, and modeling tools. *Planet. Sci. J.* **2021**, *2*, 121. [CrossRef]
116. de Batz de Trenquelléon, B.; Rosset, L.; d'Ollone, J.V.; Lebonnois, S.; Rannou, P.; Burgalat, J.; Vinatier, S. The New Titan Planetary Climate Model. I. Seasonal Variations of the Thermal Structure and Circulation in the Stratosphere. *Planet. Sci. J.* **2025**, *6*, 78. [CrossRef]
117. Gudipati, M.S.; Couturier-Tamburelli, I.; Fleury, B.; Lignell, A.; Jacovi, R. Photochemical Evolution of Condensed Organics in Titan's Atmosphere and on the Surface. In *Astrobiology Science Conference 2015 (AbSciCon 2015): Habitability, Habitable Worlds, and Life*; USRA Houston: Chicago, IL, USA, 2015.
118. Dubois, D.; Gudipati, M.S.; Henderson, B.; Carrasco, N.; Fleury, B.; Couturier-Tamburelli, I. Photochemistry of HCN Ice on Tholins Simulated in Titan's Lower Atmosphere Conditions. *EPSC 2017* **2017**, *11*, 9–10.
119. Couturier-Tamburelli, I.; Piétri, N.; Gudipati, M. Simulation of Titan's atmospheric photochemistry Formation of non-volatile residue from polar nitrile ices. *Astron. Astrophys.* **2015**, *578* , A111. [CrossRef]
120. Couturier-Tamburelli, I.; Piétri, N.; Letty, V.L.; Chiavassa, T.; Gudipati, M. UV–Vis Light-induced Aging of Titan's Haze and Ice. *Astrophys. J.* **2018**, *852*, 117. [CrossRef]
121. Mouzay, J. ; Henry, K.; Couturier-Tamburelli, I.; Danger, G.; Piétri, N.; Chiavassa, T. Photochemistry of benzene (C6H6) hydrogen cyanide (HCN) co-condensed ices part 1: A source of solid-state production of volatile nitrile compounds in Titan's stratosphere. *Icarus* **2021**, *368*, 114595. [CrossRef]
122. Wilson, E.H.; Atreya, S.K. Current state of modeling the photochemistry of Titan's mutually dependent atmosphere and ionosphere. *J. Geophys. Res. E Planets* **2004**, *109*. [CrossRef]
123. Hébrard, E.; Dobrijevic, M.; Loison, J.C.; Bergeat, A.; Hickson, K.M. Neutral production of hydrogen isocyanide (HNC) and hydrogen cyanide (HCN) in Titan's upper atmosphere. *Astron. Astrophys.* **2012**, *541*, A21. [CrossRef]
124. Hickson, K.M.; Loison, J.C.; Cavalié, T.; Hébrard, E.; Dobrijevic, M. The evolution of infalling sulfur species in Titan's atmosphere. *Astron. Astrophys.* **2014**, *572*, A58. [CrossRef]
125. Loison, J.C.; Hébrard, E.; Dobrijevic, M.; Hickson, K.M.; Caralp, F.; Hue, V.; Gronoff, G.; Venot, O.; Bénilan, Y. The neutral photochemistry of nitriles, amines and imines in the atmosphere of Titan. *Icarus* **2015**, *247*, 218–247. [CrossRef]
126. Dobrijevic, M.; Loison, J.C.; Hickson, K.M.; Gronoff, G. 1D-coupled photochemical model of neutrals, cations and anions in the atmosphere of Titan. *Icarus* **2016**, *268*, 313–339. [CrossRef]
127. Mukundan, V.; Bhardwaj, A. A Model for Negative Ion Chemistry in Titan's Ionosphere. *Astrophys. J.* **2018**, *856*, 168. [CrossRef]
128. Fox, J.L.; Yelle, R.V. Hydrocarbon ions in the ionosphere of Titan. *Geophys. Res. Lett.* **1997**, *24*, 2179–2182. [CrossRef]
129. Lavvas, P.; Yelle, R.V.; Koskinen, T.; Bazin, A.; Vuitton, V.; Vigren, E.; Galand, M.; Wellbrock, A.; Coates, A.J.; Wahlund, J.E.; et al. Aerosol growth in Titan's ionosphere. *Proc. Natl. Acad. Sci. USA* **2013**, *110*, 2729–2734. [CrossRef]
130. Loison, J.C.; Dobrijevic, M.; Hickson, K.M.; Heays, A.N. The photochemical fractionation of oxygen isotopologues in Titan's atmosphere. *Icarus* **2017**, *291*, 17–30. [CrossRef]
131. Nixon, C.A.; Bézard, B.; Cornet, T.; Coy, B.P.; de Pater, I.; Es-Sayeh, M.; Hammel, H.B.; Lellouch, E.; Lombardo, N.A.; López-Puertas, M.; et al. The atmosphere of Titan in late northern summer from JWST and Keck observations. *Nat. Astron.* **2025**, *9*, 969–981. [CrossRef]
132. Atreya, S.; Donahue, T. Ionospheric models of Saturn, Uranus, and Neptune. *Icarus* **1975**, *24*, 358–362. [CrossRef]
133. Atreya, S.K.; Romani, P.N. Photochemistry and Clouds of Jupiter, Saturn and Uranus. *Recent Adv. Planet. Meteorol.* **1985**, *17*, 68.
134. Chandler, M.O.; Waite, J.H. The Ionosphere of Uranus: A Myriad of Possibilities. *Geophys. Res. Lett.* **1986**, *13*, 6–9. [CrossRef]
135. Atreya, S.K. *Atmospheres and Ionospheres of the Outer Planets and Their Satellites*; Springer Science & Business Media: Berlin/Heidelberg, Germany, 1986; Volume 15.
136. Pollack, J.B.; Rages, K.; Pope, S.K.; Tomasko, M.G.; Romani, P.N.; Atreya, S.K. Nature of the stratospheric haze on Uranus: Evidence for condensed hydrocarbons. *J. Geophys. Res. Space Phys.* **1987**, *92*, 15037–15065. [CrossRef]
137. Waite, J.H.; Cravens, T.E. Current Review of the Jupiter, Saturn, and Uranus Ionospheres. *Adv. Space Res.* **1987**, *7*, 119–134 . [CrossRef]
138. Atreya, S.K. Uranus Photochemistry and Prospects for Voyager 2 at Neptune. *Adv. Space Res* **1990**, *10*, 119. [CrossRef]

139. Trafton, L.M.; Geballe, T.R.; Miller, S.; Tennyson, J.; Ballester, G.E. Detection of H3+ from Uranus. *Astrophys. J.* **1993**, *405*, 761–766. [CrossRef]
140. Moses, J.I.; Fouchet, T.; Bézard, B.; Gladstone, G.R.; Lellouch, E.; Feuchtgruber, H. Photochemistry and diffusion in Jupiter's stratosphere: Constraints from ISO observations and comparisons with other giant planets. *J. Geophys. Res. Planets* **2005**, *110*, E08001. [CrossRef]
141. Strobel, D.F. Photochemistry in outer solar system atmospheres. *Space Sci. Rev.* **2005**, *116*, 155–170. [CrossRef]
142. Loison, J.C.; Dobrijevic, M.; Hickson, K.M. The photochemical production of aromatics in the atmosphere of Titan. *Icarus* **2019**, *329*, 55–71. [CrossRef]
143. Melin, H.; Fletcher, L.N.; Stallard, T.S.; Miller, S.; Trafton, L.M.; Moore, L.; O'Donoghue, J.; Vervack, J.J.; Russo, N.D.; Lamy, L.; et al. The H_3^+ ionosphere of Uranus: Decades-long cooling and local-time morphology. *Philos. Trans. R. Soc. A Math. Phys. Eng. Sci.* **2019**, *377*, 20180408. [CrossRef]
144. Pentsak, E.O.; Murga, M.S.; Ananikov, V.P. Role of Acetylene in the Chemical Evolution of Carbon Complexity. *ACS Earth Space Chem.* **2024**, *8*, 798–856. [CrossRef]
145. Joshi, S.; Roth, L.; Gladstone, R.; Ivchenko, N.; Pryor, W.; Lamy, L. Uranus-hydrogen upper atmosphere: Insights from pre- and post-equinox HST Lyman-α images. *Astron. Astrophys.* **2025**, *693*, A231. [CrossRef]
146. Dobrijevic, M.; Loison, J.C.; Hue, V.; Cavalié, T.; Hickson, K.M. 1D photochemical model of the ionosphere and the stratosphere of Neptune. *Icarus* **2020**, *335*, 113375. [CrossRef]
147. Guillot, T. Condensation of Methane, Ammonia, and Water and the Inhibition of Convection in Giant Planets. *Science* **1995**, *269*, 1697–1699. [CrossRef] [PubMed]
148. Leconte, J.; Selsis, F.; Hersant, F.; Guillot, T. Condensation-inhibited convection in hydrogen-rich atmospheres: Stability against double-diffusive processes and thermal profiles for Jupiter, Saturn, Uranus, and Neptune. *Astron. Astrophys.* **2017**, *598*, A98. [CrossRef]
149. Rannou, P.; Coutelier, M.; Rivière, E.; Lebonnois, S.; Rey, M.; Maltagliati, L. Convection behind the Humidification of Titan's Stratosphere. *Astrophys. J.* **2021**, *922*, 239. [CrossRef]
150. Dobrijevic, M.; Loison, J.C.; Hickson, K.M.; Dobrijevic, M.; Loison, J.C.; Hickson, K.M. The eddy diffusion coefficient in the atmosphere of Titan: Models comparison. 2016, *Unpublished paper*. [CrossRef]
151. Petrie, S.; Bohme, D.K. Ions in space. *Mass Spectrom. Rev.* **2007**, *26*, 258–280. [CrossRef] [PubMed]
152. Arumainayagam, C. Photochemistry. In *Encyclopedia of Astrobiology*; Springer: Berlin/Heidelberg, Germany, 2022; pp. 1–6. [CrossRef]
153. Arumainayagam, C.R. Radiation Chemistry. In *Encyclopedia of Astrobiology*; Springer: Berlin/Heidelberg, Germany, 2022; pp. 1–6. [CrossRef]
154. Regina, A.; Paranjothy, M. Theoretical Investigation of Bimolecular Carbon Chain Growth Reactions in the Interstellar Media. *J. Phys. Chem.* **2023**, *128*, 2409–2416. [CrossRef]
155. Dobrijevic, M.; Hébrard, E.; Loison, J.C.; Hickson, K.M. Coupling of oxygen, nitrogen, and hydrocarbon species in the photochemistry of titan's atmosphere. *Icarus* **2014**, *228*, 324–346. [CrossRef]
156. Hrodmarsson, H.R.; Aleman, I.; Candian, A.; Wiersma, S.; Palotás, J.; Dubois, D.; Sidhu, A.; Loru, D.; Sundarajan, P.; Sciamma-O'Brien, E.; et al. The AstroPAH 10 Years of Science Review. *Space Sci. Rev.* **2025**, *221*, 42. [CrossRef]
157. Pimblott, S.M.; LaVerne, J.A. Production of low-energy electrons by ionizing radiation. *Radiat. Phys. Chem.* **2007**, *76*, 1244–1247. [CrossRef]
158. Arumainayagam, C.R.; Lee, H.L.; Nelson, R.B.; Haines, D.R.; Gunawardane, R.P. Low-energy electron-induced reactions in condensed matter. *Surf. Sci. Rep.* **2010**, *65*, 1–44. [CrossRef]
159. Shulenberger, K.E.; Zhu, J.L.; Tran, K.; Abdullahi, S.; Belvin, C.; Lukens, J.; Peeler, Z.; Mullikin, E.; Cumberbatch, H.M.; Huang, J.; et al. Electron-Induced Radiolysis of Astrochemically Relevant Ammonia Ices. *ACS Earth Space Chem.* **2019**, *3*, 800–810. [CrossRef]
160. Wu, Q.T.; Anderson, H.; Watkins, A.K.; Arora, D.; Barnes, K.; Padovani, M.; Shingledecker, C.N.; Arumainayagam, C.R.; Battat, J.B. Role of Low-Energy (<20 eV) Secondary Electrons in the Extraterrestrial Synthesis of Prebiotic Molecules. *ACS Earth Space Chem.* **2024**, *8*, 79–88. [CrossRef] [PubMed]
161. Boyer, M.C.; Rivas, N.; Tran, A.A.; Verish, C.A.; Arumainayagam, C.R. The role of low-energy ($\leq$20 eV) electrons in astrochemistry. *Surf. Sci.* **2016**, *652*, 26–32. [CrossRef]
162. Stelmach, K.B.; Neveu, M.; Vick-Majors, T.J.; Mickol, R.L.; Chou, L.; Webster, K.D.; Tilley, M.; Zacchei, F.; Escudero, C.; Flores Martinez, C.L.; et al. Secondary Electrons as an Energy Source for Life. *Astrobiology* **2018**, *18*, 73–85. [CrossRef]
163. TP, R.K.; Bjornsson, R.; Barth, S.; Ingólfsson, O. Formation and decay of negative ion states up to 11 eV above the ionization energy of the nanofabrication precursor $HFeCo_3$ (CO) $_{12}$. *Chem. Sci.* **2017**, *8*, 5949–5952. [CrossRef]
164. Ryszka, M.; Alizadeh, E.; Li, Z.; Ptasińska, S. Low-energy electron-induced dissociation in gas-phase nicotine, pyridine, and methyl-pyrrolidine. *J. Chem. Phys.* **2017**, *147*, 094303. [CrossRef]

165. Bredehöft, J.H. Electron-induced chemistry in the condensed phase. *Atoms* **2019**, *7*, 33. [CrossRef]
166. Larsson, M.; Geppert, W.D.; Nyman, G. Ion chemistry in space. *Rep. Prog. Phys.* **2012**, *75*, 066901. [CrossRef]
167. Arumainayagam, C.R. ; Garrod, R.T.; Boyer, M.; Hay, A.; Tong Bao, S.; Campbell, J.; Wang, A.; Nowak, C.M.; Arumainayagam, M.R.; Hodge, P.J. Extraterrestrial Prebiotic Molecules: Photochemistry vs. Radiation Chemistry of Interstellar Ices. *Chem. Soc. Rev.* **2019**, *48*, 2293–2314. [CrossRef]
168. Jackson, W.; Halpern, J.B.; Lin, C.S. Multiphoton ultraviolet photochemistry. *Chem. Phys. Lett.* **1978**, *55*, 254–258. [CrossRef]
169. Jackson, W.M.; Bao, Y.; Urdahl, R.S. Implications of C2H photochemistry on the modeling of C2 distributions in comets. *J. Geophys. Res. Planets* **1991**, *96*, 17569–17572. [CrossRef]
170. Carney, T.E.; Baer, T. The mechanism for multiphoton ionization of H2S. *J. Chem. Phys.* **1981**, *75*, 4422–4429. [CrossRef]
171. Achiba, Y.; Sato, K.; Shobatake, K.; Kimura, K. The mechanism for photofragmentation of H2S revealed by multiphoton ionization photoelectron spectroscopy. *J. Chem. Phys.* **1982**, *77*, 2709–2714. [CrossRef]
172. Ashfold, M.; Dixon, R. Multiphoton ionisation spectroscopy of H2S: A reinvestigation of the 1B1-1A1 band at 139.1 nm. *Chem. Phys. Lett.* **1982**, *93*, 5–10. [CrossRef]
173. Chacko, R.; Barik, S.; Banhatti, S.; Aravind, G. Multiphoton ionization and dissociation of polycyclic aromatic hydrocarbon molecules of astrophysical interest. *Phys. Rev. A* **2022**, *105*, 032804. [CrossRef]
174. Menzel, D.; Gomer, R. Electron-impact desorption of carbon monoxide from tungsten. *J. Chem. Phys.* **1964**, *41*, 3329–3351. [CrossRef]
175. Gans, B.; Boyé-Péronne, S.; Broquier, M.; Delsaut, M.; Douin, S.; Fellows, C.E.; Halvick, P.; Loison, J.C.; Lucchese, R.R.; Gauyacq, D. Photolysis of methane revisited at 121.6 nm and at 118.2 nm: Quantum yields of the primary products, measured by mass spectrometry. *Phys. Chem. Chem. Phys.* **2011**, *13*, 8140. [CrossRef]
176. Boduch, P.; Dartois, E.; De Barros, A.L.; Da Silveira, E.F.; Domaracka, A.; Lv, X.Y.; Palumbo, M.E.; Pilling, S.; Rothard, H.; Duarte, E.S.; et al. Radiation effects in astrophysical ices. *J. Phys. Conf. Ser.* **2015**, *629*, 012008. [CrossRef]
177. Hrušák, J.; Paidarová, I. Step Towards Modeling the Atmosphere of Titan: State-Selected Reactions of O^+ with Methane. *Orig. Life Evol. Biosph.* **2016**, *46*, 419–424. [CrossRef]
178. Gudipati, M.S.; Jacovi, R.; Couturier-Tamburelli, I.; Lignell, A.; Allen, M. Photochemical activity of Titan's low-altitude condensed haze. *Nat. Commun.* **2013**, *4*, 1648. [CrossRef]
179. Boyer, M.; Atkinson, K.E.; Arumainayagam, C.R. *Low-Energy Electrons : Fundamentals and Applications*; Pan Stanford Publishing: Singapore, 2019; p. 417.
180. Arumainayagam, C.R.; Herbst, E.; Heays, A.N.; Mullikin, E.; Farrah, M.; Mavros, M.G. Extraterrestrial Photochemistry: Principles and Applications. In *Prebiotic Photochemistry*; The Royal Society of Chemistry: London, UK, 2021. [CrossRef]
181. Yung, Y.L.; DeMore, W.B. *Photochemistry of Planetary Atmospheres*; Oxford University Press: Oxford, UK, 1999.
182. Plane, J.M.C.; Yung, Y.L.; DeMore, W.B. Photochemistry of Planetary Atmospheres. *J. Atmos. Chem.* **2001**, *39*, 215–216. [CrossRef]
183. Trafton, L. On the possible detection of H2 in titan's atmosphere. *Astrophys. J.* **1972**, *5*, 285–293. [CrossRef]
184. Miller, S.; Achilleos, N.; Ballester, G.E.; Geballe, T.R.; Joseph, R.D.; Prangé, R.; Rego, D.; Stallard, T.; Tennyson, J.; Trafton, L.M.; et al. The role of H_3^+ in planetary atmospheres. *Philos. Trans. R. Soc. London. Ser. A Math. Phys. Eng. Sci.* **2000**, *358*, 2485–2502. [CrossRef]
185. Zhang, Y.; Ren, B.; Yang, C.L.; Wei, L.; Wang, B.; Han, J.; Yu, W.; Qi, Y.; Zou, Y.; Chen, L.; et al. Formation of H_3^+ from ethane dication induced by electron impact. *Commun. Chem.* **2020**, *3*, 160. [CrossRef] [PubMed]
186. Kwon, S.; Sandhu, S.; Shaik, M.; Stamm, J.; Sandhu, J.; Das, R.; Hetherington, C.V.; Levine, B.G.; Dantus, M. What is the Mechanism of H_3^+ Formation from Cyclopropane? *J. Phys. Chem. A* **2023**, *127*, 8633–8638. [CrossRef]
187. Melin, H.; Moore, L.; Fletcher, L.N.; Hammel, H.B.; O'Donoghue, J.; Stallard, T.S.; Milam, S.N.; Roman, M.; King, O.R.T.; Rowe-Gurney, N.; et al. Discovery of H_3^+ and infrared aurorae at Neptune with JWST. *Nat. Astron.* **2025**, *9*, 666–671. [CrossRef]
188. Waite, J.H.; Niemann, H.B.; Yelle, R.V.; Kasprzak, W.T.; Cravens, T.E.; Luhmann, J.G.; McNutt, R.L.; Ip, W.H.; Gell, D.; De La Haye, V.; et al. Ion Neutral Mass Spectrometer Results from the First Flyby of Titan. *Science* **2005**, *85*, 195–209. [CrossRef]
189. Lorenz, R.D.; Imanaka, H.; McKay, C.P.; Makel, D.; Hunter, G.P.; Trainer, M.G.; Osiander, R.; Mastandrea, A.; Barnes, J.W.; Turtle, E.P. Hydrogen sensing in Titan's atmosphere: Motivations and techniques. *Planet. Space Sci.* **2019**, *174*, 1–7. [CrossRef]
190. López-Puertas, M.; Dinelli, B.M.; Adriani, A.; Funke, B.; García-Comas, M.; Moriconi, M.L.; D'Aversa, E.; Boersma, C.; Allamandola, L.J. Large Abundances of Polycyclic Aromatic Hydrocarbons in Titan's Upper Atmosphere. *Astrophys. J.* **2013**, *770*, 132. [CrossRef]
191. Coustenis, A.; Schmitt, B.; Khanna, R.K.; Trotta, F. Plausible condensates in Titan's stratosphere from Voyager infrared spectra. *Planet. Space Sci.* **1999**, *47*, 1305–1329. [CrossRef]
192. Griffith, C.A.; Penteado, P.; Rannou, P.; Brown, R.; Boudon, V.; Baines, K.H.; Clark, R.; Drossart, P.; Buratti, B.; Nicholson, P.; et al. Evidence for a polar ethane cloud on Titan. *Science* **2006**, *313*, 1620–1622. [CrossRef]
193. Drexel, H.; Senn, G.; Fiegele, T.; Scheier, P.; Stamatovic, A.; Mason, N.J.; Märk, T.D. Dissociative electron attachment to hydrogen. *J. Phys. At. Mol. Opt. Phys.* **2001**, *34*, 1415. [CrossRef]

194. Gans, B.; Peng, Z.; Carrasco, N.; Gauyacq, D.; Lebonnois, S.; Pernot, P. Impact of a new wavelength-dependent representation of methane photolysis branching ratios on the modeling of Titan's atmospheric photochemistry. *Icarus* **2013**, *223*, 330–343. [CrossRef]
195. Hrodmarsson, H.R.; Van Dishoeck, E.F. Photodissociation and photoionization of molecules of astronomical interest: Updates to the Leiden photodissociation and photoionization cross section database. *Astron. Astrophys.* **2023**, *675*, A25. [CrossRef]
196. Gillett, F.C. Further Observations of the 8–13 Micron Spectrum of Titan. *Astrophys. J.* **1975**, *201*, 41–43. [CrossRef]
197. Hickson, K.M.; Bray, C.; Loison, J.C.; Dobrijevic, M. A Kinetic Study of the $N(^2D)$ + C_2H_4 Reaction at Low Temperature. *Phys. Chem. Chem. Phys.* **2020**, *22*, 14026–14035. [CrossRef] [PubMed]
198. Lignell, A.; Tenelanda-Osorio, L.I.; Gudipati, M.S. Visible-light photoionization of aromatic molecules in water-ice: Organic chemistry across the universe with less energy. *Chem. Phys. Lett.* **2021**, *778*, 138814. [CrossRef]
199. Coates, A.J.; Crary, F.J.; Lewis, G.R.; Young, D.T.; Waite, J.H.; Sittler, E.C. Discovery of heavy negative ions in Titan's ionosphere. *Geophys. Res. Lett.* **2007**, *34*, L22103. [CrossRef]
200. Bézard, B.; Drossart, P.; Encrenaz, T.; Feuchtgruber, H. Benzene on the Giant Planets. *Icarus* **2001**, *154*, 492–500. [CrossRef]
201. Dubois, D.; Sciamma-O'Brien, E.; Iraci, L.T.; Barth, E.; Salama, F.; Vinatier, S. C6H6 Condensation on Titan's Stratospheric Aerosols: An Integrated Laboratory, Modeling and Experimental Approach. *Proc. Int. Astron. Union* **2019**, *15*, 189–192 . [CrossRef]
202. Vuitton, V.; Yelle, R.V.; Cui, J. Formation and distribution of benzene on Titan. *J. Geophys. Res. E Planets* **2008**, *113*, 1–18. [CrossRef]
203. Mebel, A.M.; Kislov, V.V.; Kaiser, R.I. Photoinduced mechanism of formation and growth of polycyclic aromatic hydrocarbons in low-temperature environments via successive ethynyl radical additions. *J. Am. Chem. Soc.* **2008**, *130*, 13618–13629. [CrossRef] [PubMed]
204. Parker, D.S.; Wilson, A.V.; Kaiser, R.I.; Mayhall, N.J.; Head-Gordon, M.; Tielens, A.G. On the formation of silacyclopropenylidene (c-SiC2H2) and its role in the organosilicon chemistry in the interstellar medium. *Astrophys. J.* **2013**, *770*, 33. [CrossRef]
205. Esposito, V.; Alessandrini, S.; Dubois, D.; Fortenberry, R. A Catalytic Pathway for the Formation of Cyanobenzene in Nitrogen-rich Environments and the Spectroscopy of the Reactive Intermediates. *Planet. Sci. J.* **2025**, *6*, 113. [CrossRef]
206. Sanchez, R.; Ferris, J.P.; Orgel, L.E. Conditions for Purine Synthesis: Did Prebiotic Synthesis Occur at Low Temperatures? *Science* **1966**, *36*, 677–686. [CrossRef]
207. Gupta, S.; Ochiai, E.; Ponnamperuma, C. Organic synthesis in the atmosphere of Titan. *Nature* **1981**, *293*, 725–727. [CrossRef]
208. Khare, B.N.; Sagan, C.; Zumberge, J.E.; Sklarew, D.S.; Nagy, B. Organic solids produced by electrical discharge in reducing atmospheres: Tholin molecular analysis. *Icarus* **1981**, *48*, 290–297. [CrossRef]
209. Scattergood, T.W.; McKay, C.P.; Borucki, W.J.; Giver, L.P.; van Ghyseghem, H.; Parris, J.E.; Miller, S.L. Production of organic compounds in plasmas: A comparison among electric sparks, laser-induced plasmas, and UV light. *Icarus* **1989**, *81*, 413–428. [CrossRef]
210. Thompson, W.R.; Henry, T.J.; Schwartz, J.M.; Khare, B.N.; Sagan, C. Plasma discharge in N_2 + CH_4 at low pressures: Experimental results and applications to Titan. *Icarus* **1991**, *90*, 57–73. [CrossRef]
211. McDonald, G.D.; Reid Thompson, W.; Heinrich, M.; Khare, B.N.; Sagan, C. Chemical Investigation of Titan and Triton Tholins. *Icarus* **1994**, *108*, 137–145. [CrossRef] [PubMed]
212. Coll, P.; Coscia, D.; Gazeau, M.C.; de Vanssay, E.; Guillemin, J.C.; Raulin, F. Organic chemistry in Titan's atmosphere: New data from laboratory simulations at low temperature. *Adv. Space Res.* **1995**, *16*, 93–103. [CrossRef] [PubMed]
213. Navarro-González, R.; Ramírez, S.I. Corona discharge of Titan's troposphere. *Adv. Space Res.* **1997**, *19*, 1121–1133. [CrossRef] [PubMed]
214. Ramirez, S.; Coll, P.; da Silva, A.; Navarro-González, R.; Lafait, J.; Raulin, F. Complex Refractive Index of Titan's Aerosol Analogues in the 200–900 nm Domain. *Icarus* **2002**, *156*, 515–529. [CrossRef]
215. Imanaka, H.; Khare, B.N.; Elsila, J.E.; Bakes, E.L.O.; McKay, C.P.; Cruikshank, D.P.; Sugita, S.; Matsui, T.; Zare, R.N. Laboratory experiments of Titan tholin formed in cold plasma at various pressures: Implications for nitrogen-containing polycyclic aromatic compounds in Titan haze. *Icarus* **2004**, *168*, 344–366. [CrossRef]
216. Ramírez, S.I.; Navarro-González, R.; Coll, P.; Raulin, F. Organic chemistry induced by corona discharges in Titan's troposphere: Laboratory simulations. *Adv. Space Res.* **2005**, *36*, 274–280. [CrossRef]
217. Szopa, C.; Cernogora, G.; Boufendi, L.; Correia, J.J.; Coll, P. PAMPRE: A dusty plasma experiment for Titan's tholins production and study. *Planet. Space Sci.* **2006**, *54*, 394–404. [CrossRef]
218. Ricketts, C.L.; Contreras, C.S.; Walker, R.L.; Salama, F. The coupling of a reflectron time-of-flight mass spectrometer with a cosmic simulation chamber: A powerful new tool for laboratory astrophysics. *Intern. J. Mass Spectrom.* **2011**, *300*, 26–30. [CrossRef]
219. Carrasco, N.; Gautier, T.; Es-Sebbar, E.T.; Pernot, P.; Cernogora, G. Volatile products controlling Titan's tholins production. *Icarus* **2012**, *219*, 230–240. [CrossRef]
220. Hörst, S.M.; Tolbert, M.A. In situ measurements of the size and density of titan aerosol analogs. *Astrophys. J. Lett.* **2013**, *770*, L10. [CrossRef]

221. Sciamma-O'Brien, E.; Ricketts, C.L.; Salama, F. The Titan haze simulation experiment on cOsmic: Probing titan's atmospheric chemistry at low temperature. *Icarus* **2014**, *243*, 325–336. [CrossRef]
222. Cunha De Miranda, B.; Garcia, G.A.; Gaie-Levrel, F.; Mahjoub, A.; Gautier, T.; Fleury, B.; Nahon, L.; Pernot, P.; Carrasco, N. Molecular Isomer Identification of Titan's Tholins Organic Aerosols by Photoelectron/photoion Coincidence Spectroscopy Coupled to VUV Synchrotron Radiation. *J. Phys. Chem. A* **2016**, *120*, 6529–6540. [CrossRef]
223. Dubois, D.; Carrasco, N.; Petrucciani, M.; Vettier, L.; Tigrine, S.; Pernot, P. In situ investigation of neutrals involved in the formation of Titan tholins. *Icarus* **2019**, *317*, 182–196. [CrossRef]
224. Dubois, D.; Carrasco, N.; Jovanovic, L.; Vettier, L.; Gautier, T.; Westlake, J. Positive ion chemistry in an N_2-CH_4 plasma discharge: Key precursors to the growth of Titan tholins. *Icarus* **2020**, *338*, 113437. [CrossRef]
225. Perrin, Z.; Carrasco, N.; Chatain, A.; Jovanovic, L.; Vettier, L.; Ruscassier, N.; Cernogora, G. An Atmospheric Origin for HCN-Derived Polymers on Titan. *Processes* **2021**, *9*, 965. [CrossRef]
226. He, C.; Serigano, J.; Hörst, S.M.; Radke, M.; Sebree, J.A. Titan Atmospheric Chemistry Revealed by Low-Temperature N2–CH4 Plasma Discharge Experiments. *ACS Earth Space Chem.* **2022**, *6*, 2295–2304. [CrossRef]
227. Dodonova, N.Y. Activation of nitrogen by vacuum ultraviolet radiation. *Russ. J. Phys. Chem.* **1966**, *40*, 523.
228. Sagan, C.; Khare, B.N. Experimental Jovian Photochemistry: Initial Results. *Astrophys. J.* **1971**, *15*, 563–569. [CrossRef]
229. Chang, S.; Scattergood, T.; Aronowitz, S.; Flores, J. Organic Chemistry on Titan. *Rev. Geophys. Space Phys.* **1979**, *17*, 1923–1933. [CrossRef]
230. Ferris, J.; Tran, B.; Joseph, J.; Vuitton, V.; Briggs, R.; Force, M. The role of photochemistry in Titan's atmospheric chemistry. *Adv. Space Res.* **2005**, *36*, 251–257. [CrossRef]
231. Vuitton, V.; Doussin, J.F.; Bénilan, Y.; Raulin, F.; Gazeau, M.C. Experimental and theoretical study of hydrocarbon photochemistry applied to Titan stratosphere. *Icarus* **2006**, *185*, 287–300. [CrossRef]
232. Imanaka, H.; Smith, M.A. EUV photochemical production of unsaturated hydrocarbons: Implications to EUV photochemistry in Titan and Jovian planets. *J. Phys. Chem. A* **2009**, *113*, 11187–11194. [CrossRef]
233. Carrasco, N.; Giuliani, A.; Correia, J.J.; Cernogora, G. VUV photochemistry simulation of planetary upper atmosphere using synchrotron radiation. *J. Synchrotron Radiat.* **2013**, *20*, 587–589. [CrossRef]
234. Tigrine, S.; Carrasco, N.; Vettier, L.; Cernogora, G. A microwave plasma source for VUV atmospheric photochemistry. *J. Phys. D Appl. Phys.* **2016**, *49*, 395202. [CrossRef]
235. Gautier, T.; Sebree, J.A.; Li, X.; Pinnick, V.T.; Grubisic, A.; Loeffler, M.J.; Getty, S.A.; Trainer, M.G.; Brinckerhoff, W.B. Influence of trace aromatics on the chemical growth mechanisms of Titan aerosol analogues. *Planet. Space Sci.* **2017**, *140*, 27–34. [CrossRef]
236. Carrasco, N.; Tigrine, S.; Gavilan, L.; Nahon, L.; Gudipati, M.S. The evolution of Titan's high-altitude aerosols under ultraviolet irradiation. *Nat. Astron.* **2018**, *2*, 489–494. [CrossRef]
237. Berry, J.L.; Ugelow, M.S.; Tolbert, M.A.; Browne, E.C. Chemical Composition of Gas-Phase Positive Ions during Laboratory Simulations of Titan's Haze Formation. *ACS Earth Space Chem.* **2019**, *3*, 202–211. [CrossRef]
238. Bourgalais, J.; Carrasco, N.; Vettier, L.; Pernot, P. Low-Pressure EUV Photochemical Experiments: Insight on the Ion Chemistry Occurring in Titan's Atmosphere. *J. Geophys. Res. Space Phys.* **2019**, *124*, 9214–9228. [CrossRef]
239. Bourgalais, J.; Carrasco, N.; Vettier, L.; Comby, A.; Descamps, D.; Petit, S.; Blanchet, V.; Gaudin, J.; Mairesse, Y.; Marty, B. Aromatic Formation Promoted by Ion-Driven Radical Pathways in EUV Photochemical Experiments Simulating Titan's Atmospheric Chemistry. *J. Phys. Chem. A* **2021**, *125*, 3159–3168. [CrossRef]
240. Carrasco, N.; Bourgalais, J.; Vettier, L.; Pernot, P.; Giner, E.; Spezia, R. A missing link in the nitrogen-rich organic chain on Titan. *Astron. Astrophys.* **2022**, *663*, A165. [CrossRef]
241. Curtis, D.B.; Hatch, C.D.; Hasenkopf, C.A.; Toon, O.B.; Tolbert, M.A.; McKay, C.P.; Khare, B.N. Laboratory studies of methane and ethane adsorption and nucleation onto organic particles: Application to Titan's clouds. *Icarus* **2008**, *195*, 792–801. [CrossRef]
242. Sciamma-O'Brien, E.; Upton, K.T.; Salama, F. The Titan Haze Simulation (THS) experiment on COSmIC. Part II. Ex-situ analysis of aerosols produced at low temperature. *Icarus* **2017**, *289*, 214–226. [CrossRef]
243. Couturier-Tamburelli, I.; Toumi, A.; Piétri, N.; Chiavassa, T. Behaviour of solid phase ethyl cyanide in simulated conditions of Titan. *Icarus* **2018**, *300*, 477–485. [CrossRef]
244. Fleury, B.; Gudipati, M.S.; Couturier-Tamburelli, I.; Carrasco, N. Photoreactivity of condensed acetylene on Titan aerosols analogues. *Icarus* **2019**, *321*, 358–366. [CrossRef]
245. Selliez, L.; Maillard, J.; Cherville, B.; Gautier, T.; Thirkell, L.; Gaubicher, B. High resolution mass spectrometry for future space missions: Comparative analysis of complex organic matter with LAb- CosmOrbitrap and LDI-FTICR. *Rapid Commun. Mass Spectrom.* **2019**, *34*, e8645. [CrossRef]
246. Mouzay, J.; Couturier-Tamburelli, I.; Piétri, N.; Chiavassa, T. Experimental simulation of Titan's stratospheric photochemistry: benzene (C_6H_6) ices. *J. Geophys. Res. Planets* **2020**, *126*, e2020JE006566. [CrossRef]
247. Couturier-Tamburelli, I. ; Danger, G.; Mouzay, J.; Piétri, N. Photochemistry of benzene (C_6H_6) hydrogen cyanide (HCN) co-condensed ices part 2: Formation of aerosols analogues of titan's atmosphere. *Icarus* **2025**, *438*, 116626. [CrossRef]

248. Imanaka, H.; Smith, M.A. Role of photoionization in the formation of complex organic molecules in Titan's upper atmosphere. *Geophys. Res. Lett.* **2007**, *34*, 1–5. [CrossRef]
249. Thissen, R.; Vuitton, V.; Lavvas, P.; Lemaire, J.; Dehon, C.; Dutuit, O.; Smith, M.A.; Turchini, S.; Catone, D.; Yelle, R.V.; et al. Laboratory studies of molecular growth in the titan ionosphere. *J. Phys. Chem. A* **2009**, *113*, 11211–11220. [CrossRef] [PubMed]
250. Peng, Z.; Gautier, T.; Carrasco, N.; Pernot, P.; Giuliani, A.; Mahjoub, A.; Correia, J.J.; Buch, A.; Bénilan, Y.; Szopa, C.; et al. Titan's atmosphere simulation experiment using continuum UV-VUV synchrotron radiation. *J. Geophys. Res. Planets* **2013**, *118*, 778–788. [CrossRef]
251. Tigrine, S.; Carrasco, N.; Bozanic, D.K.; Garcia, G.A.; Nahon, L. FUV Photoionization of Titan Atmospheric Aerosols. *Astrophys. J.* **2018**, *867*, 164. [CrossRef]
252. Anderson, C.M.; Samuelson, R.E.; Mclain, J.L.; Dworkin, J.P. The SPECTRAL Ice Chamber: Application to Titan's Stratospheric Ice Clouds. *Astrophys. J.* **2018**, *865*, 62. [CrossRef]
253. Sciamma-O'Brien, E.; Roush, T.L.; Rannou, P.; Dubois, D.; Salama, F. First Optical Constants of Laboratory-generated Organic Refractory Materials (Tholins) Produced in the NASA Ames COSmIC Facility from the Visible to the Near Infrared (0.4–1.6 μm): Application to Titan's Aerosols. *Planet. Sci. J.* **2023**, *4*, 121 . [CrossRef]
254. Hudson, R.L.; Yarnall, Y.Y.; Gerakines, P.A. Benzene Vapor Pressures at Titan Temperatures: First Microbalance Results. *Planet. Sci. J.* **2022**, *3*, 121. [CrossRef]
255. Coupeaud, A.; Kołos, R.; Aycard, J.P.; Pie, N. Photochemical Synthesis of the Cyanodiacetylene HC_5N: A Cryogenic Matrix Experiment. *J. Phys. Chem.* **2006**, *110*, 2371–2377. [CrossRef] [PubMed]
256. Couturier-Tamburelli, I.; Piétri, N.; Crépin, C.; Turowski, M.; Guillemin, J.C.; Kołos, R. Synthesis and spectroscopy of cyanotriacetylene (HC7N) in solid argon. *J. Chem. Phys.* **2014**, *140*, 044329. [CrossRef] [PubMed]
257. Mouzay, J.; Piétri, N.; Couturier-Tamburelli, I.; Chiavassa, T. UV irradiation of benzene in N2 matrix: A relevant study for titan's chemistry. *J. Mol. Struct.* **2021**, *1237*, 130296. [CrossRef]
258. Carrasco, N.; Dutuit, O.; Thissen, R.; Banaszkiewicz, M.; Pernot, P. Uncertainty analysis of bimolecular reactions in Titan ionosphere chemistry model. *Planet. Space Sci.* **2007**, *55*, 141–157. [CrossRef]
259. Carrasco, N.; Pernot, P. Modeling of branching ratio uncertainty in chemical networks by dirichlet distributions. *J. Phys. Chem. A* **2007**, *111*, 3507–3512. [CrossRef]
260. Carrasco, N.; Alcaraz, C.; Dutuit, O.; Plessis, S.; Thissen, R.; Vuitton, V.; Yelle, R.; Pernot, P. Sensitivity of a Titan ionospheric model to the ion-molecule reaction parameters. *Planet. Space Sci.* **2008**, *56*, 1644–1657. [CrossRef]
261. Heays, A.N.; Bosman, A.D.; Van Dishoeck, E.F. Photodissociation and photoionisation of atoms and molecules of astrophysical interest. *Astron. Astrophys.* **2017**, *602*, A105 . [CrossRef]
262. Zhou, J.; Zhao, Y.; Hansen, C.S.; Yang, J.; Chang, Y.; Yu, Y.; Cheng, G.; Chen, Z.; He, Z.; Yu, S.; et al. Ultraviolet photolysis of H2S and its implications for SH radical production in the interstellar medium. *Nat. Commun.* **2020**, *11*, 1547. [CrossRef]
263. Chang, Y.; Ashfold, M.N.; Yuan, K.; Yang, X. Exploring the vacuum ultraviolet photochemistry of astrochemically important triatomic molecules. *Natl. Sci. Rev.* **2023**, *10*, nwad158. [CrossRef] [PubMed]
264. Hager, T.J.; Moore, B.M.; Borengasser, Q.D.; Renshaw, K.T.; Johnson, R.; Kanaherarachchi, A.C.; Broderick, B.M. VUV Processing of Nitrile Ice: Direct Comparison of Branching in Ice and TPD Spectra. *Acs Earth Space Chem.* **2025**. [CrossRef]
265. Mebel, A.M.; Hayashi, M.; Jackson, W.M.; Wrobel, J.; Green, M.; Xu, D.; Lin, S.H. Branching ratios of C_2 products in the photodissociation of C_2H at 193 nm. *J. Chem. Phys.* **2001**, *114*, 9821–9831. [CrossRef]
266. Loison, J.C.; Bergeat, A.; Caralp, F.; Hannachi, Y. Rate constants and H atom branching ratios of the gas-phase reactions of methylidyne CH(X2II) radical with a series of alkanes. *J. Phys. Chem. A* **2006**, *110*, 13500–13506. [CrossRef]
267. Carrasco, N.; Plessis, S.; Pernot, P. Towards a reduction of the bimolecular reaction model for Titan ionosphere. *Int. J. Chem. Kinet.* **2008**, *40*, 699–709. [CrossRef]
268. Lilensten, J.; Witasse, O.; Simon, C.; Soldi-Lose, H.; Dutuit, O.; Thissen, R.; Alcaraz, C. Prediction of a N_2^{++} layer in the upper atmosphere of Titan. *Geophys. Res. Lett.* **2005**, *32*, 1–4. [CrossRef]
269. Thissen, R.; Witasse, O.; Dutuit, O.; Wedlund, C.S.; Gronoff, G.; Lilensten, J. Doubly-charged ions in the planetary ionospheres: A review. *Phys. Chem. Chem. Phys.* **2011**, *13*, 18264. [CrossRef]
270. Matsubara, T. A model of ionization-induced reactions in CH_4/N_2 clusters in Titan's atmosphere: Theoretical insights into mono- and divalent states. *Bull. Chem. Soc. Jpn.* **2024**, *97*, uoae047. [CrossRef]
271. Matsubara, T. Theoretical Insights into a Novel Ion-Ion Reaction of Methane in the Initial Stages of Hydrocarbon Growth in Space. *Acs Earth Space Chem.* **2024**, *8*, 2557–2573. [CrossRef]
272. Hargreaves, J. The Solar-Terrestrial Environment. In *The Solar-Terrestrial Environment*; Springer: Berlin/Heidelberg, Germany, 1995.
273. Chaizy, P.; Rème, H.; Sauvaud, J.A.; d'Uston, C.; Lin, R.P.; Larson, D.E.; Mitchell, D.L.; Anderson, K.A.; Carlson, C.W.; Korth, A.; et al. Negative ions in the coma of comet Halley. *Nature* **1991**, *349*, 393–396. [CrossRef]
274. Coates, A.J.; Jones, G.H.; Lewis, G.R.; Wellbrock, A.; Young, D.T.; Crary, F.J.; Johnson, R.E.; Cassidy, T.A.; Hill, T.W. Negative ions in the Enceladus plume. *Icarus* **2010**, *206*, 618–622. [CrossRef]

275. Coates, A.J.; Wellbrock, A.; Lewis, G.R.; Jones, G.H.; Young, D.T.; Crary, F.J.; Waite, J.H. Heavy negative ions in Titan's ionosphere: Altitude and latitude dependence. *Planet. Space Sci.* **2009**, *57*, 1866–1871. [CrossRef]
276. Wellbrock, A.; Coates, A.J.; Jones, G.H.; Lewis, G.R.; Waite, J.H. Cassini CAPS-ELS observations of negative ions in Titan's ionosphere: Trends of density with altitude. *Geophys. Res. Lett.* **2013**, *40*, 4481–4485. [CrossRef]
277. Desai, R.T.; Coates, A.J.; Wellbrock, A.; Vuitton, V.; Crary, F.J.; González-Caniulef, D.; Shebanits, O.; Jones, G.H.; Lewis, G.R.; Waite, J.H.; et al. Carbon chain anions and the growth of complex organic molecules in Titan's ionosphere. *Astrophys. J. Lett.* **2017**, *844*, L18 . [CrossRef]
278. Vuitton, V.; Lavvas, P.; Yelle, R.V.; Galand, M.; Wellbrock, A.; Lewis, G.R.; Coates, A.J.; Wahlund, J.E. Negative ion chemistry in Titan's upper atmosphere. *Planet. Space Sci.* **2009**, *57*, 1558–1572. [CrossRef]
279. Marif, H.; Lilensten, J. Suprathermal electron moments in the ionosphere. *J. Space Weather Space Clim.* **2020**, *10*, 22. [CrossRef]
280. Wang, Z.; Su, Z.; Liu, N.; Dai, G.; Zheng, H.; Wang, Y.; Wang, S. Suprathermal Electron Evolution Under the Competition Between Plasmaspheric Plume Hiss Wave Heating and Collisional Cooling. *Geophys. Res. Lett.* **2020**, *47*, e2020GL089649. [CrossRef]
281. Millar, T.J.; Walsh, C.; Field, T.A. Negative ions in space. *Chem. Rev.* **2017**, *117*, 1765–1795. [CrossRef]
282. Martinez, O.; Yang, Z.; Demarais, N.J.; Snow, T.P.; Bierbaum, V.M. Gas-phase reactions of hydride anion, H-. *Astrophys. J.* **2010**, *720*, 173–177. [CrossRef]
283. Pirim, C.; Gann, R.; McLain, J.; Orlando, T. Electron-molecule chemistry and charging processes on organic ices and Titan's icy aerosol surrogates. *Icarus* **2015**, *258*, 109–119. [CrossRef]
284. Harada, N.; Herbst, E. Modeling Carbon Chain Anions in L1527. *Astrophys. J.* **2008**, *685*, 272–280. [CrossRef]
285. Rawat, P.; Prabhudesai, V.S.; Rahman, M.; Ram, N.B.; Krishnakumar, E. Absolute cross sections for dissociative electron attachment to NH_3 and CH_4. *Int. J. Mass Spectrom.* **2008**, *277*, 96–102. [CrossRef]
286. Mackay, G.I.; Betowski, L.D.; Payzant, J.D.; Schiff, I.; Bohme, D.K. Proton-Transfer Reactions with HCN and CH3CN Rate Constants at 297 K for Proton-Transfer Reactions with HCN and CH3CN. Comparisons with Classical Theories and Exothermicity. *J. Phys. Chem.* **1976**, *80*, 2919–2922. [CrossRef]
287. Barckholtz, C.; Snow, T.P.; Bierbaum, V.M. Reactions of Cn- and CnH- with Atomic and Molecular Hydrogen. *Astrophys. J.* **2001**, *547*, 171–174. [CrossRef]
288. Herbst, E.; Osamura, Y. Calculations on the Formation Rates and Mechanisms for CnH Anions in Interstellar and Circumstellar Media. *Astrophys. J.* **2008**, *679*, 1670. [CrossRef]
289. Yang, Z.; Cole, C.A.; Martinez, O., Jr.; Carpenter, M.Y.; Snow, T.P.; Bierbaum, V.M. Experimental and Theoretical Studies of Reactions Between H Atoms and Nitrogen-Containing Carbanions. *Astrophys. J.* **2011**, *739*, 19. [CrossRef]
290. Itikawa, Y.; Mason, N. Cross sections for electron collisions with water molecules. *J. Phys. Chem. Ref. Data* **2005**, *34*, 1–22. [CrossRef]
291. Horvath, G.; Aranda-Gonzalvo, Y.; Mason, N.J.; Zahoran, M.; Matejcik, S. Negative ions formed in $N_2/CH_4/Ar$ discharge—A simulation of Titan's atmosphere chemistry. *Eur. Phys. J. Appl. Phys.* **2009**, *49*, 13105. [CrossRef]
292. Dubois, D.; Carrasco, N.; Bourgalais, J.; Vettier, L.; Desai, R.; Wellbrock, A.; Coates, A. Nitrogen-containing Anions and Tholin Growth in Titan's Ionosphere: Implications for Cassini CAPS-ELS Observations. *Astrophys. J. Lett.* **2019**, *872*, L31. [CrossRef]
293. Dubois, D.; Sciamma-O'Brien, E.; Fortenberry, R. The Fundamental Vibrational Frequencies and Spectroscopic Constants of the Dicyanoamine Anion, $NCNCN^-$ ($C_2N_3^-$): Quantum Chemical Analysis for Astrophysical and Planetary Environments. *Astrophys. J.* **2019**, *883*, 109. [CrossRef]
294. Bierbaum, V.M. Anions in Space and in the Laboratory. *Proc. Int. Astron. Union* **2011**, *7*, 383–389. [CrossRef]
295. Capone, L.A.; Whitten, R.C.; Prasad, S.S.; Dubach, J. The ionospheres of Saturn, Uranus, and Neptune. *Astrophys. J.* **1977**, *215*, 977–983. [CrossRef]
296. Romani, P.N.; Atreya, S.K. Methane Photochemistry and Haze Production on Neptune. *Icarus* **1988**, *74*, 424–445. [CrossRef]
297. Bezard, B.; Feuchtgruber, H.; Encrenaz, T. *Observations of Hydrocarbons in the Giant Planets*; The Universe as Seen by ISO: Paris, France, 1999.
298. Mao, M.; Benedikt, J.; Consoli, A.; Bogaerts, A. New pathways for nanoparticle formation in acetylene dusty plasmas: A modelling investigation and comparison with experiments. *J. Phys. D Appl. Phys.* **2008**, *41*, 225201. [CrossRef]
299. Krishnakumar, E.; Denifl, S.; Cadez, I.; Markelj, S.; Mason, N.J. Dissociative electron attachment cross sections for H_2 and D_2. *Phys. Rev. Lett.* **2011**, *106*, 243201. [CrossRef]
300. Song, M.Y.; Yoon, J.S.; Cho, H.; Karwasz, G.P.; Kokoouline, V.; Nakamura, Y.; Tennyson, J. Cross sections for electron collisions with acetylene. *J. Phys. Chem. Ref. Data* **2017**, *46*, 013106. [CrossRef]
301. Čadež, I.; Markelj, S.; Rupnik, Z. Low energy H^- production by electron collision with small hydrocarbons. *Eur. Phys. J. D* **2012**, *66*, 73. [CrossRef]
302. Szymańska, E.; Mason, N.J.; Krishnakumar, E.; Matias, C.; Mauracher, A.; Scheier, P.; Denifl, S. Dissociative electron attachment and dipolar dissociation in ethylene. *Int. J. Mass Spectrom.* **2014**, *365–366*, 356–364. [CrossRef]

303. Janečková, R.; May, O.; Fedor, J. Dissociative electron attachment to methylacetylene and dimethylacetylene: Symmetry versus proximity. *Phys. Rev. A—At. Mol. Opt. Phys.* **2012**, *86*, 052702. [CrossRef]
304. May, O.; Fedor, J.; Ibănescu, B.C.; Allan, M. Absolute cross sections for dissociative electron attachment to acetylene and diacetylene. *Phys. Rev. A—At. Mol. Opt. Phys.* **2008**, *77*, 040701. [CrossRef]
305. May, O.; Kubala, D.; Allan, M. Absolute cross sections for dissociative electron attachment to HCN and DCN. *Phys. Rev. A* **2010**, *82*, 010701. [CrossRef]
306. Tanzer, K.; Pelc, A.; Huber, S.E.; Czupyt, Z.; Denifl, S. Low energy electron attachment to cyanamide (NH2CN) Low energy electron attachment to cyanamide (NH_2CN). *J. Chem. Phys.* **2015**, *142* , 034301. [CrossRef]
307. Pelc, A.; Huber, S.E.; Matias, C.; Czupyt, Z.; Denifl, S. Formation of Negative Ions upon Dissociative Electron Attachment to the Astrochemically Relevant Molecule Aminoacetonitrile. *J. Phys. Chem. A* **2016**, *120*, 903–910. [CrossRef]
308. Fiquet-Fayard, F.; Ziesel, J.P.; Azria, R.; Tronc, M.; Chiari, J. Formation of HS^- and DS^- by Dissociative Attachment in H2S, HDS, and D2S. *J. Chem. Phys.* **1972**, *56*, 2540–2548. [CrossRef]
309. Rao, M.V.V.S.; Srivastava, S.K. Electron Impact Ionization and Attachment Cross Sections for H_2S. *J. Geophys. Res.* **1993**, *98*, 13137–13145. [CrossRef]
310. Simon, A.; Cohen, I.; Hedman, M.; Hofstadter, M.; Mandt, K.; Nimmo, F. Uranus Flagship Science-Driven Tour Design: Community Input Poll. *arXiv* **2025**, arXiv:2505.05514. [CrossRef]